Developments in Measuring Enhancement and Quenching of Optical Nonlinearities from Gold Nanoantennas

Honors Thesis by

Nicholas D. Entin

Department of Physics, University of Colorado, Boulder, CO 80309, USA

Thesis Advisor: Markus B. Raschke (Department of Physics)
Honors Council Representative: John P. Cumalat (Department of Physics)
Outside Reader: Divya E. Vernerey (Department of Mathematics)

A thesis submitted for partial fulfilment of the degree of Bachelor of Arts in Physics with Honors Distinction

Defense Date: March 29th, 2023

To my mother, father, and sister for supporting me no matter how big my goals and no matter how weird my interests.

Acknowledgements

I am truly thankful for the people that are around me today and the people that supported me to become who I am as a scientist and as a person. I want to acknowledge my mother and father for doing their best to teach me about the world and support my interests. I am sure it was not easy raising a kid who would not stop talking about space, dinosaurs, and rocks, but having the freedom to explore the things that made me happy is what allowed me to discover physics and my many other passions. For that, I am forever grateful.

In the Raschke group, I first want to thank Dr. Wenjin Luo for being a wonderful collaborator, mentor, and teacher for my research projects, and for teaching me about academia and physics research in general. I would not have learned all of the content and technical skills I have now without him, and I will carry this experience for the rest of my career. He was always in lab to help me troubleshoot. I also want to thank Professor Markus Raschke for giving me the opportunity to work in this amazing research group while pursuing my undergraduate degree and for all of the support in this project. I always felt rewarded by his teachings and encouraged by his confidence. Through these mentorships, I learned many amazing things that have helped me become a better physicist, and I feel ready to take on graduate school. I want to specifically thank Benjamin Whetten for always being willing to talk through and help me with my project, and Dr. Fabian Menges for his early mentorship and support. Finally, I would also like to thank all of the members of the Raschke group for providing support and help with nearly 3 years of ongoing research: Roland Wilcken, Emily Chavez, Yueying Wang, Richard Puro, Fatema Fairooz, Sam Turner, Branden Esses, John Altenhofen, Nate Londres and former members Kathryn Hasz, Andreij Gadelha, Vasily Kravtsov, and Peter Lande.

I would like to acknowledge my thesis committee members Professor John Cumalat for his mentorship and feedback in my honors project and Professor Divya Vernerey for her support with my mathematics degree and life advice that I will keep close to me after graduating. I would like to acknowledge the Boettcher Foundation for granting a scholarship to cover my tuition, fees, books, housing, and living expenses while I was in college. The financial stability provided by this scholarship allowed me to pursue research without having to worry about working an extra job to make ends meet. Finally, I would like to acknowledge my partner, Eleanor Gentry, and closest friends at the University of Colorado Boulder: Robi Huq, Sophie Redd, Morgan Knuesel, Megan Finnigan, Mason Divita, Taylor Henderson, Sanjay Kumar Keshava, Sam Lippincott, Ryan Hamilton, and Matt Brown. Thank you all for your friendship, kindness, and humor. I could not have imagined a better circle of peers to go on this college journey with me.

Contents

Abstract

Nonlinear nano-optics, which studies light-matter interactions in various materials and nanostructures, is a rapidly developing topic of research. Over the last decade, researchers have made incredible strides in exploring novel optical regimes involving the localization of electromagnetic fields to only a few nanometers and the corresponding dramatic enhancement of nonlinear optical effects. As scientists begin to unravel the mysteries of light-matter interactions on a nanoscale, many questions about nonlinear optical responses in metallic nanostructures remain unanswered.

In Au nanostructures, the optical response from intraband electronic transitions give rise to efficient nonlinear emissions, including the third-order coherent four-wave mixing (FWM) and second-order incoherent hot electron luminescence (HEL). Observations of spectral shift and near-field enhancement of nonlinear emissions have been observed for few nanometer distances, and deviations from the classical predictions are attributed to quantum effects. However, there is debate regarding the nanostructure coherent and incoherent near-field light-matter interaction and how it is modified by quantum effects at small interparticle separations.

Here, I will discuss the necessary background and foundational tools for experiments that will provide more insight on the quantum processes driving the emission mechanism for FWM and HEL in Au nanostructures. The fabrication process for Au nanoantennas in these experiments is described in detail, and modifications are made to improve the nanoantenna quality. For the first time, the experimental setup and measurement protocol are described, and we make significant progress in implementing a scanning tunneling microscope (STM) to the experiment. We demonstrate a functional STM system and make key design modifications that will allow the system to be used in future investigations. Finally, we show preliminary measurements and analysis methods that will contribute to understanding the coherent and incoherent near-field light-matter interaction at small interparticle separations. In addition to reviewing the motivational experiments and scientific analysis of successful measurements, the results of this thesis serve as a valuable resource for future experiments by putting past protocols on paper and establishing foundational work to addressing the open science questions.

1 Introduction

Understanding optical nonlinearities in nanostructures is key for developing novel *nanospectroscopy* methods and *optical information processing*. Novel *nanospectroscopy* methods allow many different fields of science, including nanotechnology, chemistry, and biochemistry, to observe materials in new ways. It is also common for the medical field to use nanospectroscopy to observe viruses, biological molecules, and cancer cells to develop new treatment methods. *Optical information processing* is a new approach to computation that could exceed the current calculation speed and communication speed of electronics by using photon-based circuits instead of electron-based circuits [1]. The development of these applications requires a deeper understanding of nonlinear optical responses [2, 3, 4].

Physicists studying atomic and molecular optics are interested in understanding emission mechanisms when light interacts with nanostructures. When light hits a material, the energy of that photon can cause electrons in the material to change energy levels. When those electrons relax from an excited state to a ground state, photons with new optical properties are emitted. When light interacts with a media that responds nonlinearly to electric fields, the emission mechanism is a nonlinear process and can result in a host of fascinating optical phenomena. In addition, when light interacts with nanostructures, external electromagnetic fields can be localized to nanoscale regions, resulting in enhanced field amplitudes and corresponding enhanced optical emissions. Nanostructures of interest mostly include nanoscale gaps and nanoantennas, and previous studies conclude that metallic nanostructures have a strong optical response as a result of the free electrons being excited inside nanoparticles [1]. As a result, incredible strides have been made in the field of ultrafast nano-optics that take advantage of this strong optical response in order to measure and better understand nonlinear signals.

When excited with visible light, gold (Au) nanostructures have efficient nonlinear optical emissions, making them an excellent candidate for investigating nonlinear light-matter

interactions. For Au nanostructures, the optical response from electronic transitions gives rise to efficient nonlinear emissions, including the coherent four-wave mixing (FWM) and incoherent hot electron luminescence (HEL) response [2]. Many researchers have used Au nanoantennas to observe these signals, but there is still scientific debate regarding the incoherent hot electron mechanism in general and the coherent emission mechanisms like FWM at nanoscale gaps.

The latest experimental and technological developments opened a gateway to increasing the efficiency of nonlinear optical emissions, allowing researchers to better measure the optical signals and observe them with different structures. Until recently, creating a variable separation between Au structures with subnanometer precision was not possible. However, recent advancements in distance control using atomic force microscopy (AFM) and scanning tunneling microscopy (STM) make this subnanometer precision possible, allowing researchers to approach a Au nanoantenna to a Au surface and study how emissions change as the separation decreases [4]. These advancements in nonlinear emission efficiency and distance control technology provide an opportunity to investigate the FWM and HEL response of Au nanostructures at the transition from large particle separations to small particle separations, where quantum tunneling electrons and near-field coupling can change the emission mechanism. While there is some established knowledge about hot electrons and coherent emission processes in Au, the standing questions about how nanoscale gaps between Au structures will affect these processes warrant further investigation of the experiments, results, and models that investigate the FWM and HEL response in Au nanostructures.

The open science questions this project investigates are as follows: (1) How does the FWM and HEL signal from a Au nanoantenna vary as a function of incident laser power, and what can we conclude about the plasmon lifetime? (2) How does the FWM and HEL signal from a Au nanoantenna vary as we approach a Au sample? (3) How is the HEL and FWM signal quenched when we get into the tunneling regime, and how does the tunneling current correlate with the FWM/HEL signals? Answering these question requires the use of femtosecond laser science and development of advanced experimental techniques with

nanometer distance control. In addition to reviewing the motivating papers and scientific analysis of successful measurements, **the goal of the research for this thesis is to put past protocols on paper and establish foundational work to addressing these open science questions**, which is valuable for future investigations.

In the "Background" portion of this thesis, I will give a brief overview of the physical framework necessary to understand the methods and related results for experiments investigating the FWM and HEL response in Au nanostructures. I will discuss two motivating papers for this research study and use them to motivate investigating the unique optical properties of these signals in nanostructures. In the "Nanoantenna Fabrication" portion of this thesis, I will discuss the process of fabricating and characterizing Au nanoantennas. This will include a detailed procedure for using electrochemistry to etch a nanoantenna, characterizing and selecting nanoantennas for experiment, mounting the nanoantennas to tuning forks for AFM, and adding a grating structure to the nanoantenna for coupling incident laser light. I will also describe improvements made to the fabrication process. In the "Experiment" portion of this thesis, I will give an overview of the optical setup and describe the protocol for measuring FWM and HEL at the apex of a nanoantenna. Additionally, I will review the operation principles of AFM and STM in experiments where the tip of the nanoantenna approaches a surface to create small tip-surface separations, and I will show the current successes in combining STM interaction with nanometer distance control and femtosecond laser science. In the "Measurement and Analysis" section, I will review successful measurements and analysis steps that establish the foundational work to understanding the emission mechanism for FWM and HEL in Au nanostructures. This includes power dependent measurements of the FWM and HEL, successes in implementing an STM, and preliminary results of the FWM signal as the Au nanoantenna approaches a Au surface. I will discuss these results, then conclude by summarizing the promising trends that warrant further investigation of the FWM and HEL signals, reiterating the necessary tools provided in this thesis for addressing the open scientific questions on the topic, and discussing future applications that could result from a deeper understanding.

2 Background

2.1 Surface Plasmon Polaritons

Surface plasmon polaritons (SPPs) are a type of surface wave with unique properties that allow for many applications in optics. A surface wave is a wave that propagates along an interface between different media. Similarly, SPPs are electromagnetic waves that propagate along a metal–dielectric interface [1]. In this experiment, the metal is Au in a nanoantenna, and the dielectric is the air around the Au [2]. The SPPs propagate along and are bound to an interface between the two media, but they have a shorter wavelength than light of the same frequency. The unique property of SPPs propagating along a surface with shorter wavelength means that SPPs have more momentum then propagating light waves, so they can be used in optics to locally enhance fields.

Surface plasmons are simply delocalized electron oscillations at a metal-dielectric interface. The surface plasmons are from oscillations of the charge density at the surface of a metal [2]. Similarly, a polariton is simply an oscillation resulting from strong coupling of electromagnetic waves with a dipole-carrying excitation. For SPPs, the surface plasmons are essentially oscillating surface charges, and these oscillating charges create a moving dipole that couples to the electromagnetic fields from the incident laser light to create polaritons [1]. Being a combination of both surface plasmons and polaritons, SPPs are essentially a new class of quasiparticles, or particle-like quantizations, propagating along the surface of a metal near the speed of light.

2.2 SPP Propagation and Nanofocusing

The SPP can be effectively confined to the surface of an interface. The spatial confinement of the surface wave depends on the media it is propagating in and the wave vector (k) of the surface plasmon. When k is sufficiently small, the SPPs can propagate along the metal-dielectric interface, but electric and magnetic fields in the SPP are not

strongly confined to the interface. On the metal side of the SPP, the spatial extent is only within skin depth of the metal, so the SPP fields are very close to the interface. On the air side of the SPP, the spatial extent is not very confined, extending beyond the wavelength of the SPP. Thus, since the SPP fields are weakly confined to the interface, there is effectively no enhancement of local fields. In contrast, when k is sufficiently large, the speed of the SPP is much smaller (wave propagation speed is $\frac{w}{k}$, where w is the frequency). Thus, phase variations of the plasmon are not considerable, and we can use quasistatic approximations for the SPP. The notable result of this is we find that, in the case of large k, SPPs and their associated fields are strongly confined to the interface. It is worth noting that because of Ohmic losses, any spatial extent of the SPP field in a metal will dampen the SPP wave. However, this dampening is much less considerable for a stronger surface confinement than for a weaker surface confinement. Further, because k for an SPP is big compared to k for a light wave with identical frequency, SPPs can be confined locally to regions far smaller than the diffraction limit of light. Thus, optical experiments that take advantage of SPPs are able to probe much smaller scales than any conventional far-field optical experiments [1].

In order to use SPPs in optical experiments, it is essential to create SPPs using incident laser light. However, because SPPs cannot radiate far-field light from a surface, far-field light hitting a metal surface alone cannot create SPPs. One option to create an SPP is to use complicated and sensitive methods using near-field light to couple incident laser light with SPPs, but working with far-field excitation schemes is much more straightforward [1]. Using special geometries, it is still possible to couple far-field light with SPPs. The most notable geometries either take advantage of total internal reflection or use a fanned grating structure to couple broadband light with SPPs by aligning the dispersion of the light and SPP [1].

SPPs can be used to "nanofocus" light to increase the emissions of nonlinear signals. Nanoantennas are particularly interesting nanostructures of Au because the metal can support an SPP mode, and the geometry causes the propagating SPP to "focus" [1]. At the start of the nanofocusing process, an SPP is generated at the fan-shaped grating

structure, which then propagates towards the tip apex. The spatial extent of SPPs can be confined to regions at the surface of a metal on the order of angstroms [1]. As a result of the conical shape of the tip and the surface confinement of the SPPs, as the SPP propagates from where it is generated to the tip apex, the wave packet at the surface becomes smaller. Essentially, the SPP is concentrated nearly adiabatically as it moves towards the apex, resulting in coherent light that is spatially confined to the apex. This means that all of the light that was coupled at the grating structure with a large surface area is confined to a nanoscale region at the apex, creating a local field enhancement [5]. Other nanofocusing geometries have also been studied, including different cones, wedges, and nanogrooves, many of which have shown similar SPP focusing effects [1]. When the propagating SPP reaches the tip apex, it can no longer propagate and is re-emitted as a photon at the tip apex. The resulting signal is emitted at the tip apex and is enhanced due to this field enhancement from the adiabatic compression [2].

2.3 Four-Wave Mixing

One nonlinear signal that is often measured from Au nanostructures is from four-wave mixing (FWM). FWM is a phenomenon in nonlinear optics that involves multiple photons. In the case of exciting Au, the interaction of three photons with different frequencies produce a photon with a new frequency, which is measured as the FWM signal. In most experiments, the excitation spectrum hitting the Au is broadband, so there are many different combinations of three frequencies that can add to create the FWM frequency. Thus, the FWM signal is broadband, but the spectral structure is defined by the spectrum of the incident excitation light [2]. From three frequencies $(\omega_1, \omega_2, \omega_3)$ picked from the broadband excitation spectrum, the frequency of the FWM response in Au is calculated as

$$\omega_{\text{FWM}} = \omega_1 - \omega_2 + \omega_3. \tag{1}$$

Figure 1 shows the possible excitation mechanisms for the FWM process. One option for

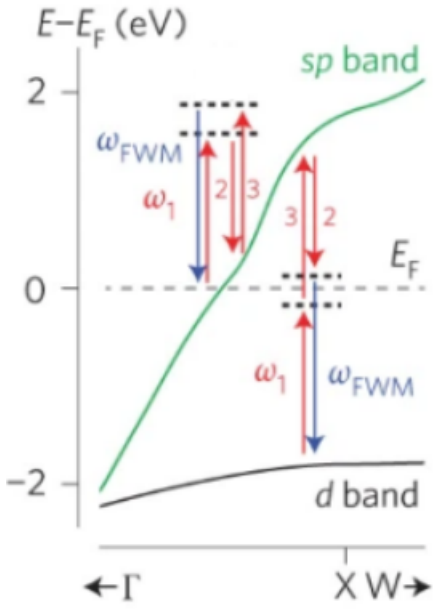

Figure 1: Band diagram of Au showing the possible mechanisms that produce the FWM signal at frequency ω_{FWM}. E is the energy of the electron, and E_F indicates the Fermi energy. The horizontal axis indicates the wave vector. Figure adapted from [3].

the FWM process involves intraband electronic transitions. For this process, the incident laser excites an electron from the *sp* band to a virtual energy level (via ω_1), back down to *sp* band (via ω_2), then up to a final energy (via ω_3). When the electron relaxes, a photon of frequency ω_{FWM} is emitted. Another option for the FWM process involves interband electronic transitions. For this process, ω_1 and ω_3 combine to excite the electron from the *d* band to the *sp* band, then the electron jumps down to a virtual energy level (via ω_2). Again, when the electron relaxes, a photon of frequency ω_{FWM} is emitted [3].

The FWM can be enhanced by nanofocusing SPPs using the process described in Section 2.2. For example, one study uses enhanced FWM to image plasmon concentrations on a Au surface as a function of time in order to investigate plasmon dynamics [3]. This experiment uses a femtosecond-pulse laser to observe plasmon dynamics on the order of femtoseconds. In addition, as a result of the spatial confinement from nanofocusing the SPP along the conical Au nanoantenna, the Au surface images achieve a spatial resolution on the order of 10 nanometers.

2.4 Hot Electron Luminescence

As mentioned above, surface plasmons are a key interest in nanophotonics because they can be used to capture large amounts of far-field light and focus it into nanometer-sized volumes far below the classical diffraction limit. However, these surface plasmons have finite lifetimes, and they will eventually decay away via two different paths. The first path, which has been discussed extensively in the previous section, involves the surface plasmon decaying radiatively into a photon, leading to enhancement of emitted signals. The second path involves nonradiative decay, where the surface plasmon decay forms electron-hole pairs, generating hot carriers [7]. The electron in this pair, often called a hot electron, is essentially an out-of-equilibrium electron from a metal that has gained a significant amount of kinetic energy from the strong electric field in regions of high field intensities [14]. The kinetic energy of hot electrons is far above the Fermi level, so the electron exists in a high-energy state. In brief, this decay channel of the surface plasmon involves creating an electron-hole pair with a high-energy electron and a low-energy hole [7].

Electron-hole pairs can recombine to create luminescence, but the exact mechanism for the luminescence in Au from hot electrons is still under debate. Often when exciting Au surfaces with infrared light and observing the optical response, there is an incoherent nonlinear broadband emission with relatively low-intensity [14]. In contrast with the FWM, which is a coherent process, this broadband emission is an incoherent nonlinear process, meaning there is no fixed phase relation between the excitation and emitted photons [2]. The signal has been attributed to be from the recombination of hot electrons, and it will be referred to as hot electron luminescence (HEL). The luminescence phenomena is often explained by high-energy conduction-band electrons recombining with low-energy d-band holes caused by a two-photon absorption into the metal, which in turn creates a nonlinear emission [14]. The broadband emission has also been measured in experiments studying Au nanostructures [2]. The unique properties of plasmons in metal nanostructures and enhancement of nonlinear signals via SPP nanofocusing continues to

fuel discussions about the origins of nonlinear luminescence like HEL in metallic nanostructures [14]. While there is still an ongoing debate about the details of the incoherent emission mechanism in Au nanostructures, most researchers agree that the electronic transitions contributing to the HEL are from within the conduction band of Au. That is, the hot electrons and holes are recombining within the conduction band (i.e. within the *sp*-band) of the metal particles in the nanostructure [2, 14].

Because the electronic transitions are within the *sp*-band of the metal, the resulting spectrum from this transition depends on the shape of the Fermi-Dirac distribution, which is temperature dependent [2]. Thus, the spectra can be approximated using a Boltzmann distribution, given by

$$I \propto e^{\frac{-\hbar(\delta\omega)}{k_B T_e}}, \tag{2}$$

where I is the intensity of the spectrum, T_e the electron temperature, $\delta\omega$ is the difference in the frequency of the two excitation photons, and $\hbar$ and k_B are fundamental constants. Thus, by inverting this formula, it is possible to calculate the hot electron temperature from the measured broadband HEL spectrum, as done in previous work [2].

The hot electrons that result from the nonradiative decay path of surface plasmons have many research interests. For instance, hot carriers can catalyze chemical reactions, suggesting that hot electrons have applications in photon-induced reactions, specifically photochemistry that could be enabled by plasmons. Further, hot electrons from surface plasmons are an avenue to convert light into electrical current, and some studies have suggested using them to create new photodetection devices or harvest solar energy [7]. However, a more complete understanding of the generation of hot electrons and how they create a measurable luminescent signal is necessary to explore these applications.

It is worth noting that the debate surrounding hot electrons in metallic nanostructures goes far beyond the details of the mechanism that contributes to a measurable spectrum. For instance, one suggested mechanism claims that the broadband emission is not from the recombination of electrons and holes at all. Instead, the emission could be a result of energy of the electron-hole pair exciting a plasmon, which in turn will emit a photon. So,

in this explanation, the incoherent nonlinear signal sometimes measured when exciting metallic nanostrucures is instead from the radiative decay path of the plasmon. Another suggested mechanism is that the signal is actually from inelastic light scattering or Raman scattering and not from the decay of a plasmon [20]. Even though SPPs can decay nonradiatively and form hot electrons, this decay path is sparsely researched compared to the radiative decay path that directly produces an optical signal. In order to better understand the mechanism that forms hot electrons and leads to HEL, and in order to realize the potential this process has as a catalyst, in photodetection technology, and in solar cells, it is imperative to collect additional data in future experiments.

2.5 Motivating Experiments

The open science questions that motivate this research project are largely inspired by two key research papers. The first paper investigates third-order optical nonlinearities in a Au nanoantenna driven by surface plasmon field gradients. The second paper investigates photoluminescence (PL) with few femtosecond radiative lifetimes of a coupled plasmonic emitter in a Au nanoantenna at the transition from the classical coupling regime to the quantum coupling regime.

The first study uses the SPP nanofocusing process with a Au nanoantenna to confine excitation fields and demonstrate higher conversion efficiency of nonlinear optical frequency mixing than ever measured previously. This study specifically looks at the enhanced third-order nonlinear four-wave mixing signal [2]. This paper also investigates the nonlinear conversion efficiency of FWM using nanofocused SPPs. In this experiment, a mask is used to filter the full broadband incident laser spectrum into two distinct frequencies, ω_1 and ω_2. Because it has a higher intensity, the peak with frequency ω_1 contributes 2 photons, and the lower intesnity ω_2 contributes 1 photon. Thus, the FWM has center frequency $\omega_{\text{FWM}} = 2\omega_1 - \omega_2$ [2]. By varying the difference between ω_1 and ω_2, this study determines that the FWM conversion efficiency is dependent on this dif-

ference and independent of the overall excitation frequency. The conversion efficiency is a measure of how well the fundamental excitation light is converted to a nonlinear signal, so a higher FWM intensity measurement corresponds to a higher conversion efficiency. Demonstrating an increase in the FWM intensity for a decrease in the difference between excitation frequencies suggests new opportunities for enhancing nonlinear signals by making careful decisions about the spectrum of the excitation laser light. Avenues to enhance nonlinear signals are essential for the future of nonlinear optical nanodevices and future nanospectroscopies [2]. The FWM is a fascinating nonlinear signal that offers many insights to investigating nonlinear optics and light-matter interactions, and the ability to enhance nonlinear signals like the FWM are critical for these investigations. Further, this paper observes an incoherent emission at the tip apex, which is attributed to hot electrons. However, this paper fails to resolve the near-field light matter coherent and incoherent interactions, and warrants further investigation of the incoherent emission from hot electrons [2].

The second study examines photoluminescence at and between the classical resonant energy transfer regime at large distances and the quantum coupling regime at small distances. For metals, the photoluminescent signal is from excited *sp* band electrons recombining with *d* band holes when the metal interacts with light. This particular study does not use the SPP nanofocusing we discussed earlier, so it does not measure the weaker nonlinear FWM and HEL. Simply by illuminating the tip apex, there is optical enhancement, but it is not as dramatic as that from the nanofocusing process since the plasmon is generated effectively at the apex. This paper specifically uses the photoluminescence spectra to determine how the plasmon resonance at the gap changes for different tip-surface distances. The experiment uses STM and shear-force atomic force microscopy (AFM) to control the distance between the tip and the surface with subnanometer resolution. This distance control is used to approach the nanoantenna to a flat surface to create a small, variable gap. This allows for the unique optical properties in that gap to be dynamically explored at classical coupling distances, quantum tunneling distances, and the transition between these two regimes.

In this study, when the tip-surface distance is large enough to ignore the effects of quantum tunneling electrons, the surface plasmons at the metallic tip apex resonate and couple with the atoms in the Au surface. The coupling between the plasmon at the tip apex and the flat Au surface can be regarded as a classical dipole resonance, which enhances the local field and leads to an associated optical signal enhancement. However, when the gap between the tip and the surface is only a few nanometers (the "quantum tunneling regime"), the charges tunnel. This leads to a reduction of the local electromagnetic field and corresponding quenching of the optical signal [4]. In summary, the emission at the gap depends on a competition between this near-field enhancement from classical plasmon coupling and optical quenching from electron tunneling effects, depending on the gap size. The study shows that the field-enhanced behavior of the photoluminescence signal dominates in a $\sim 15\,\text{nm}$ to $\sim 2\,\text{nm}$ separation until quantum coupling reduces emission intensity in a $\sim 2\,\text{nm}$ to $0\,\text{nm}$ separation [4].

2.6 Open Questions

Another study suggests that tunneling electrons would contribute to the HEL spectrum in Au nanostructures. The experiment uses a fixed 1 nm gap between a Au nanoantenna and a flat Au surface to study the enhancement of photoluminescence in the tunneling regime. A bias voltage is set between the tip and the surface, allowing for inelastic electron tunneling. The enhancement of radiative plasmon decay into an optical signal is attributed to the tunneling of hot electrons, which offers an alternative decay channel [10]. So, the ability of hot electrons to tunnel at small interparticle separations will contribute to the plasmon decay, and possibly the resulting optical signal. However, this study does not investigate if we would see enhancement and quenching of the HEL like is observed for the PL. In fact, neither the FWM signal nor the HEL signal has been investigated at the transition from the classical coupling to quantum tunneling regime, so it is unknown if either would demonstrate optical enhancement and quenching like the

photoluminescence signal in Au nanostructures.

We are motivated by two main ideas. The first paper introduces how we can create the FWM and HEL signal at a tip apex using a grating structure on a Au nanoantenna. It discusses nanofocusing SPPs to enhance these signals, and leaves some questions about the HEL. Further review of present research reveals that there are still many questions regarding the HEL. The second paper introduces how we can create an interparticle gap that allows for the quantum tunneling of electrons by bringing the tip apex within a few nanometers of a sample. Previous knowledge about how plasmon dynamics change at quantum scales and how electron tunneling can attenuate the optical signal leads us to question how the FWM and HEL signal from a Au nanoantenna varies as we approach a flat Au sample. Further, are these signals quenched when we get into the tunneling regime, and how does the tunneling current correlate? These are challenging questions to address, which will require the development of advanced experimental techniques with femtosecond laser science and precision control. The remainder of this thesis will be dedicated to establishing the foundation work in fabrication, experiment design, and experimental protocols to addressing these open science questions, which will undoubtedly be valuable for future investigations.

3 Nanoantenna Fabrication

An essential part of this experiment is the fabrication of Au nanoantennas, or "tips". Commercial measurement devices exist that use these tips for different measurements, such as atomic force microscopy (AFM) or scanning tunneling microscopy (STM). Often, these tips can be manufactured on a large scale and sold commercially. However, for unique experimental setups that are on the forefront of nanospectroscopy research, there are custom components that require custom-made tips. The fabrication process is sensitive, and many careful details need to be considered to improve the quality of the tips. The procedure described in this section includes many steps that were determined

through many trials to improve the quality of the tips.

3.1 Electrochemical Etching

To start, the conical shape of the tips is made using electrochemistry. A fully detailed procedure was written for future reference, which will be stored in the laboratory and used by future researchers. In summary, a small ring made of platinum wire is connected to the negative terminal of a power supply, then the ring is placed slightly below the surface of a solution of 50% HCl and 50% ethanol. The ring is parallel to the surface of the solution, and platinum is chosen due to its conductivity and chemical inertness. A small segment of 125 µm diameter Au wire is straightened and connected to the positive terminal. The wire is placed into the solution a few millimeters below the platinum ring, perpendicular to the surface of the solution and in the center of the platinum ring. An image of the apparatus is shown in Figure 2.

Figure 2: A closup view of the tip-etching apparatus, showing the Au wire in an etching solution, perpendicular to the solution surface and in the center of a platinum ring.

When a voltage is applied between the Au wire and the platinum ring, the Au will begin to etch away and dissolve into the solution at the surface. As the Au etches away, the wire becomes an hourglass shape at the surface of the solution. When the diameter of the wire at the surface of the solution becomes small enough, the weight of the Au wire that is submerged in the solution will cause the submerged part to fall off. As the

submerged wire falls off, it will pull the Au wire with it until it breaks away. This process forms the conical structure with a sharp tip that is desired. With the Au wire no longer submerged in the solution, the voltage falls to 0, and the etching process is complete. A diagram of this process is shown in Figure 3.

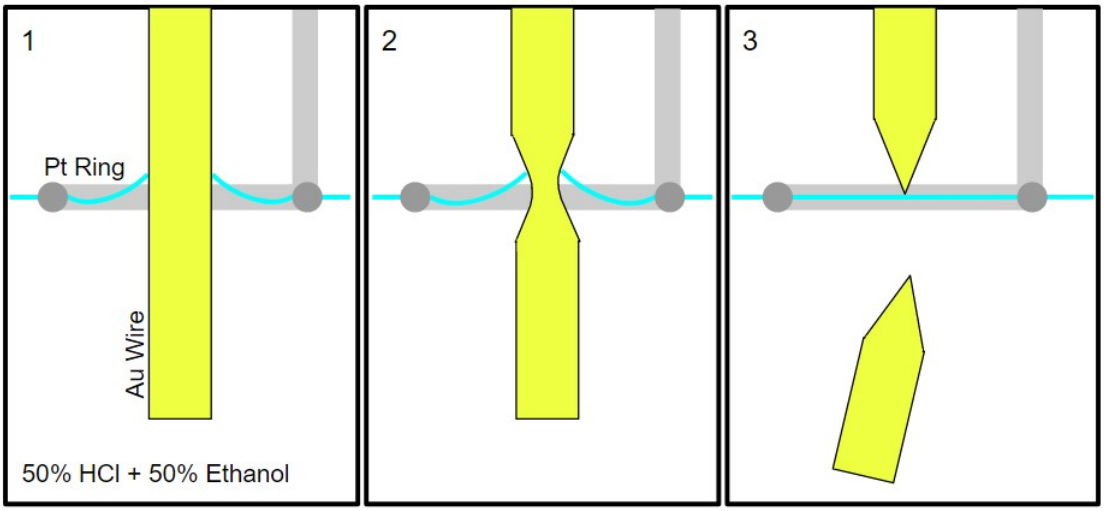

Figure 3: Diagram of the tip etching process. Panel 1 shows the initial configuration of the Au wire and Pt ring in an etching solution. Panel 2 shows the Au etching away after a voltage is applied between the ring and the wire. Panel 3 shows the submerged portion of the wire breaking off, leaving a sharp tip above the surface. Figure created by author.

The tip can then be removed from the solution, cut near the base (about 1 cm from the apex), and placed in a sample box. It is important to avoid touching the sharp tip to any surface or debris, as the structure is very fragile and can easily be damaged. As a first test, the tip apex is observed under an optical microscope to check for any bending or surface features that would make the tip not usable for experiment. The fabrication process is prone to error, even when precautions are taken such as limiting floor vibrations during etching, wearing gloves, and making the tips under a fume hood. These external factors can contribute to rough surfaces on the sides of the cone and a tip apex that bends and is not straight in the direction of the wire. Overall, frequent cleaning of the materials and tools used in the etching procedure and careful alignment of the wire (i.e. making sure the Au wire is orthogonal and the platinum ring is parallel to the solution surface) yields a more sharp tip apex and a more smooth cone.

The quality of the tip matters for experiments, which is why so much caution and

characterization needs to occur. If the apex of the tip is not sharp, then the nanofocusing process described in Section 2.2 will result in less local field enhancement due to a larger region at the apex. This will, in turn, result in a weaker optical signal at the apex. If the sides of the cone are not smooth, then the SPP can emit as a photon before the apex at a rough surface feature. This will result in a weaker optical signal at the apex because of a lower conversion efficiency of the SPP into the emitted signal at the apex. So, in order to maximize the strength of the optical signal we want to measure at the apex, the tips have to be both sharp and smooth.

After mounting the tips onto a small tuning fork, which is described in Section 3.2, the tips can be observed and characterized using a scanning electron microscope (SEM). An SEM produces images of a sample by scanning a focused beam of electrons over the surface. The electrons interact with atoms in the sample and are backscattered into an electron detector, which can be used to determine the surface topography with nanometer resolution. Not only does the SEM allow us to see how smooth the surface of the cone is, but it also allows us to directly measure the size of the tip apex. From many attempts to measure the FWM and HEL, it is determined that a tip suitable for experimentation has an apex diameter of about 20 - 30 nm. Unfortunately, the beam of electrons used in an SEM can damage the tip apex, so the SEM can only be used to observe the apex for a small duration of time, or it can be used to characterize tips that will not be used in an experiment. An example of a tip that is suitable for experiment is included in Figure 4.

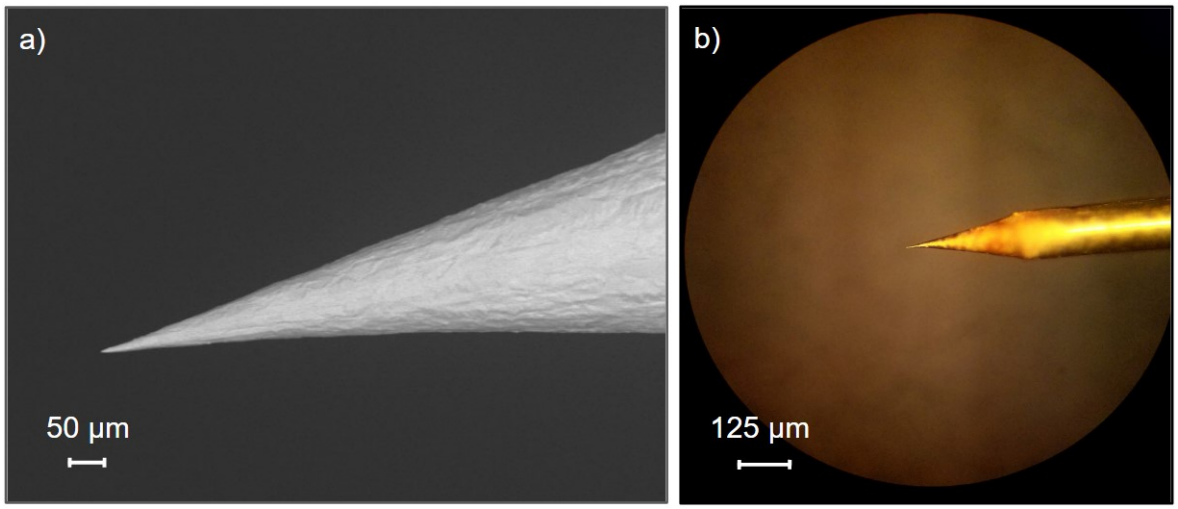

Figure 4: a) SEM image and b) optical image of an example tip that is suitable for experimentation. The optical image is from a 5x magnification under an optical microscope. Figure created by author.

3.2 Mounting and Grating

After the tips are electrochemically etched, they must be mounted onto a small tuning fork so they can be used for shear-force atomic force microscopy (AFM). AFM is described in brief in Section 4.3. The tuning fork type crystals are a common electronic component used as a clock source in time management applications such as communication equipment, measuring instruments, and microprocessors. For this application, we use a quartz tuning fork with a 32.768 kHz crystal with lateral dither piezo excitation for shear-force tip-sample distance control [4]. The tuning fork is typically contained within a metal cylinder, so it must first be carefully removed from the cylinder. Each leg of the tuning fork is connected to a wire lead, and each wire lead must be bent in two places so that the tuning fork will fit into the pre-designed mount in the experiment. An image of the prepared tuning fork is included in Figure 5.

Each Au tip is on the end of a ∼1 cm length of Au wire. The tip is carefully placed onto a bit of sticky tape on a microscope slide with the apex hanging over the edge of the slide. Under an optical microscope, a razor blade is then used to cut the excess wire from the tip so that there is enough wire to glue to the base of the tip to the tuning fork with the tip apex extending slightly beyond the end of the tuning fork. Using a thin

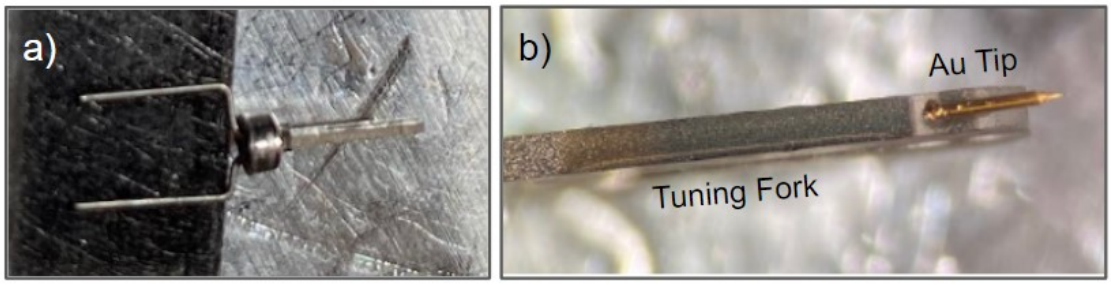

Figure 5: Example of a) prepared tuning fork and b) tuning fork with properly glued Au tip. Figure created by author.

wire as an application tool, a small drop of ultraviolet curing optical adhesive is applied to the quartz pad at the end of the tuning fork farthest from the base. The wire side of the tip is then picked up using tweezers and placed on the drop of adhesive, and the tip is aligned to be parallel to the length of the tuning fork. When only using the tip for AFM, it is very important to maintain electrical contact between the Au tip and the metal pad of the tuning fork that is farthest from the base. This is because the tip needs to be grounded to avoid unwanted electronic forces between the tip and a sample. An image of a properly cut tip glued to the proper pad of the tuning fork is shown in Figure 5. The tuning fork and tip apparatus can then be placed in a Petri dish and put under an ultraviolet light so the adhesive can cure.

After the tips are properly mounted to the tuning fork, a focused ion beam (FIB) is used to add a fanned grating structure to the surface of the cone. The FIB uses Ga+ ions to mill away the surface of a material inside of a vacuum chamber. The exact parameters and details of the fanned grating structure, including the spacing, angles, width, and depth of the gratings that optimize the conversion from incident laser light to SPPs, are described in [5]. As described in Section 2.2, the grating structure is used to couple the incident laser light with the Au and generate an SPP, which then propagates towards the tip apex. What wavelength of light that can couple with the material at the grating is related to the spacing between the gaps, so in brief, the fan-shaped grating structure is used so a broadband laser spectrum can be coupled with the Au and generate a broadband SPP [5]. The small wavelengths of the broadband incident laser spectrum couple where the gaps are close together, and the large wavelengths couple where the

gaps are farther apart. Another reason that the tip needs to be in electrical contact with the tuning fork is that the wire lead of the tuning fork can easily be grounded during the FIB milling process. If the tip is not grounded, hitting the surface with ions will cause charge buildup and excessive milling. An SEM image of the tip after the grating has been added is included in Figure 6.

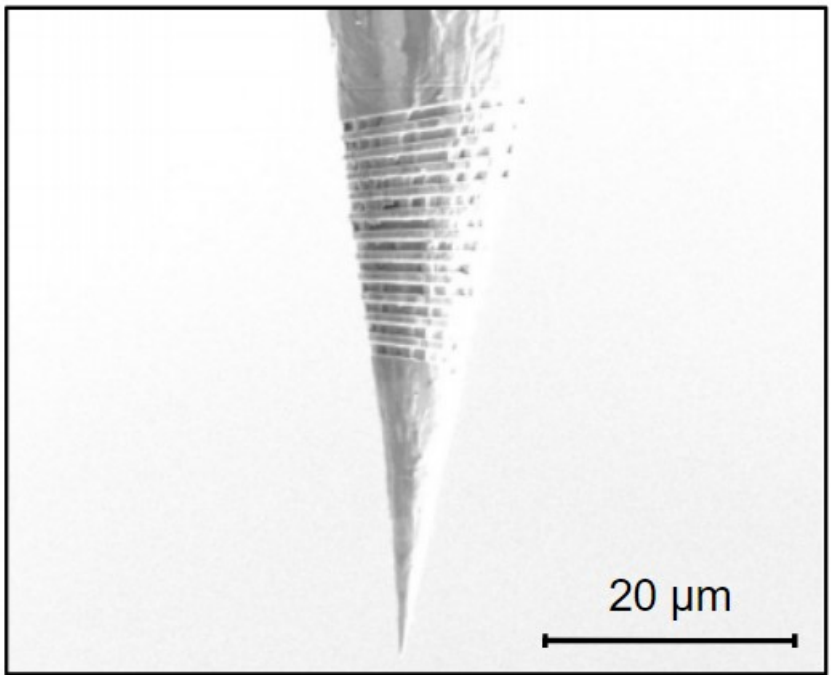

Figure 6: SEM image of the Au nanoantenna after a fanned grating structure is added to the side using a FIB. Figure created by author.

3.3 Improvements to the Nanoantenna Fabrication Process

As described in the previous section, etching Au tips is a very laborious and sensitive process. Many external factors can contribute to slight variations in the final product. For example, if the etching solution has contaminants or if the applied voltage is noisy, the cone could have a rough surface. Further, if the Au wire is not perfectly perpendicular to the solution, then when the submerged wire falls off, it will pull the Au at an angle, resulting in a bent/curved tip apex that is not parallel with the axis of the cone. Vibrations around the tip etching setup can also cause these defects. Further, the exact

mechanics of how the submerged wire falls off and pulls the Au into a sharp apex depends heavily on minute environmental factors that are difficult to control. As mentioned in Section 3.1, the quality of a tip significantly effects how useful it is in these experiments, as a tip with a dull apex, bent apex, and/or rough surface will result in a weaker optical signal at the apex.

Out of every batch of 10-20 tips etched, it was found that almost half of the tips had a dull apex, a bent apex, and/or a rough surface. Thus, these tips were usually discarded, as they could not be reliably used for experiment. The FWM and HEL can be difficult signals to measure, so significant effort was made to increase the tip quality in order to increase the yield of tips that can be used to measure these inherently weak signals. To start, simple precautions are taken during the procedure, including limiting floor vibrations during etching, frequently changing gloves, and making the tips under a fume hood. In order to assure that the applied voltage was as expected in the solution, we used Au-plated alligator clips to hold onto the Au wire and the Pt ring.

The most significant modification made to the tip etching process was adding a step to anneal the Au wire before electrochemically etching it into a nanoantenna. The wire is pre-cut into $\sim$10 cm segments, then it is placed in a furnace, heated to 800 °C for 8 hours, then allowed to slowly cool to room temperature. The wire has a visibly smoother surface after annealing. The annealing process is a heat treatment that alters the physical properties of the Au. As the wire slowly cools down, the Au atoms are allowed to solidify in a more uniform crystalline structure than before. When the annealed wire is electrochemically etched, the etching will stay along the lattice structures, which results in a much more smooth cone surface. Figure 7 shows an example of a tip etched from normal wire and a tip etched from the annealed wire. Overall, it was determined that tips from the annealed wire are more likely to have a smoother surface and a sharper apex. Before we used annealed wire to make the tips, about 1 in 10 tips could be used to measure the FWM signal. When these new annealed tips were used in experiments, we found that we could measure the FWM signal in about 1 in 3 tips, which is a significant improvement. Installing a new tip, aligning the incident laser beam, and determining if

a tip can be used to measure the FWM signal can take several hours. Not only does this better yield decrease the waste from unusable tips, but it also decreases the amount of time it takes to perform a successful measurement.

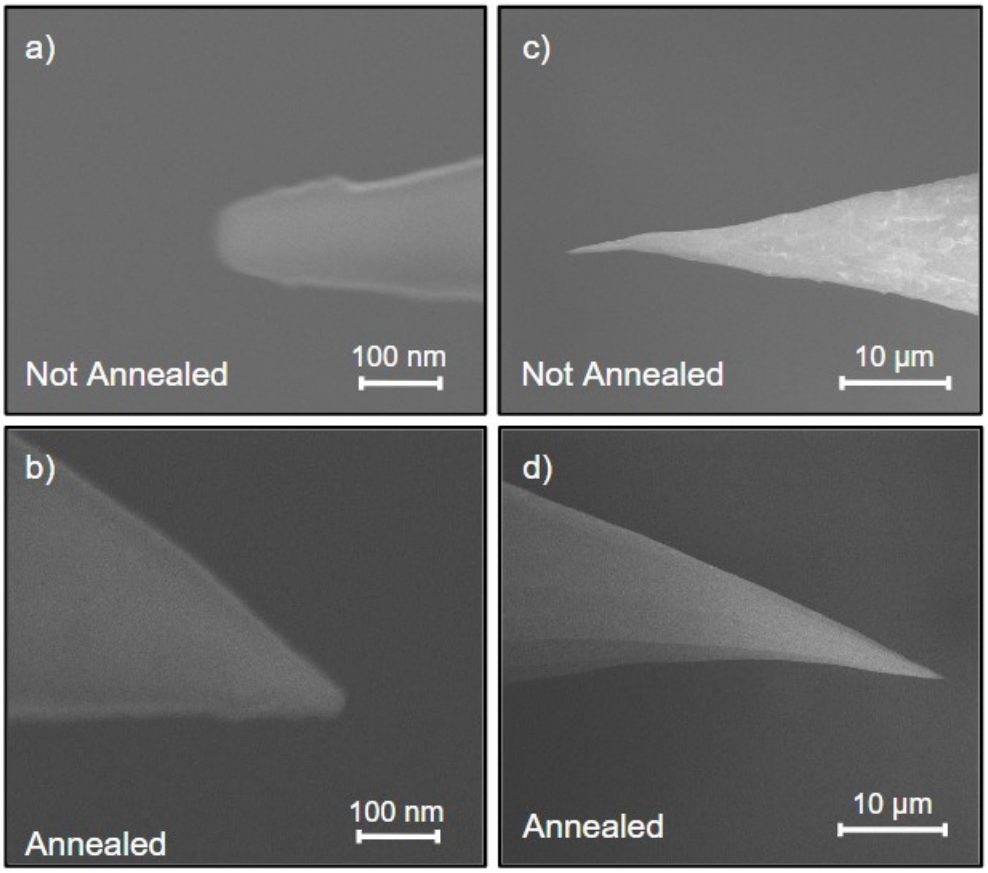

Figure 7: SEM images of the tip apex from the a) non-annealed wire and b) annealed wire at a 100 nm scale, showing a sharper apex for the annealed wire. SEM images of the tip surface from the c) non-annealed wire and d) annealed wire at a 10 µm scale, showing a smoother surface for the annealed wire. Figure created by author.

4 Experiment

4.1 Overview

In this experiment, we measure the FWM and HEL signal generated in a Au nanoantenna with a ∼10 nm apex radius. We use adiabatic nanofocusing and detect a spatially filtered emission at the apex to spatially confine the excitation fields and eliminate background signals. The complete optical setup is included in Figure 8, which also includes a

simplified diagram. For this experiment, we use broadband pulses from a Ti:Sa oscillator with center wavelength ∼800 nm, bandwidth FWHM ∼100 nm, pulse duration ∼10 fs, pulse energy ∼8 nJ, and repetition rate 80 MHz (Femtolasers Synergy). Inherent laser instability causes a change in the relative phase of different wavelengths in the spectrum. The incoming pulse may be linearly chirped or present higher order group delay dispersion (GDD). Chirp is a sudden change of the center wavelength of a laser. Un-chirped light has a stronger intensity, so there is a stronger nonlinear response if the incident light is unchirped. The pulses from the Ti:Sa laser are shaped in amplitude and phase using a spatial light modulator (SLM) to remove the chirp.

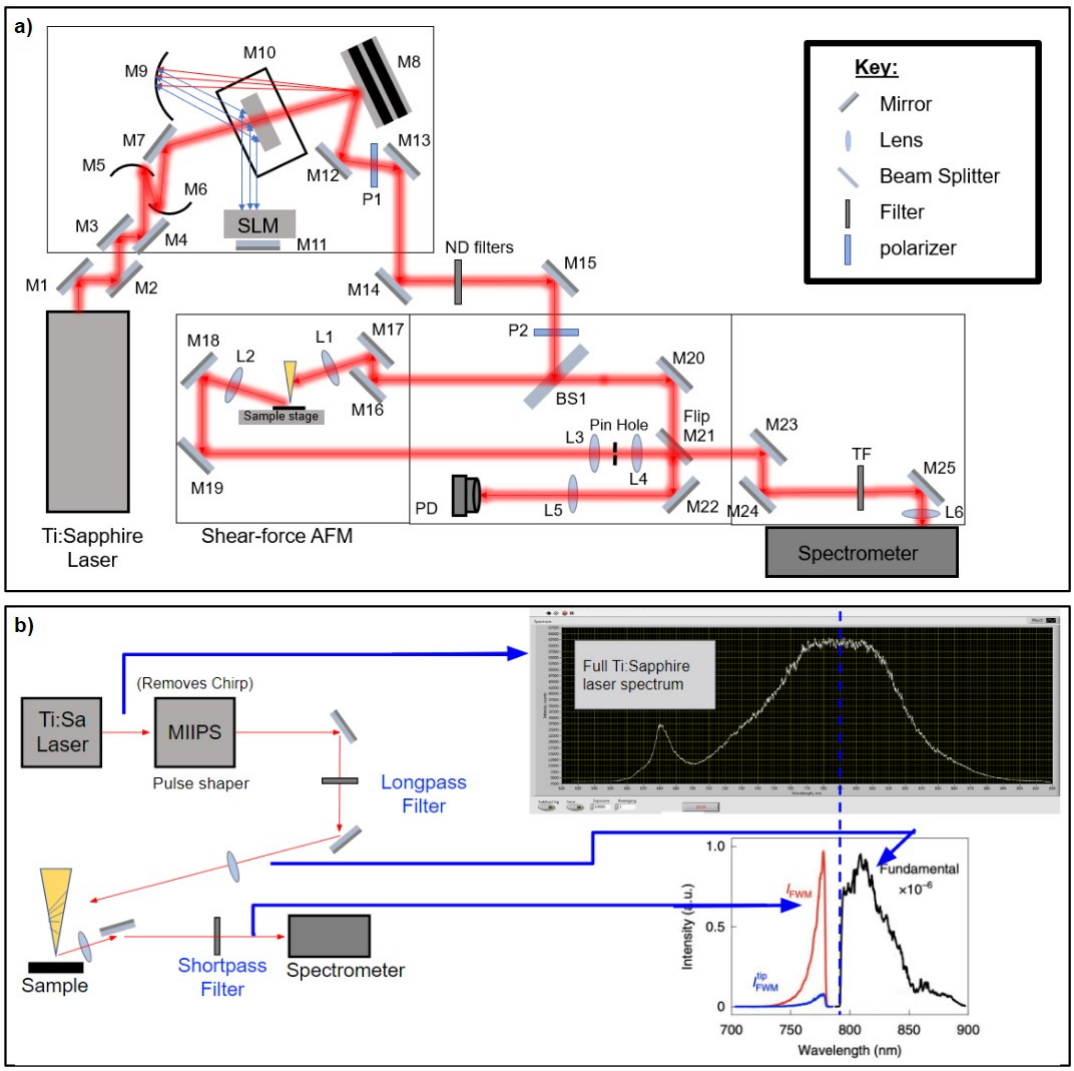

Figure 8: a) Complete system setup. Figure created by Wenjin Luo. b) Simplified system setup for reference. Figure created by author.

Multiphoton intrapulse interference phase scan (MIIPS) is a method used in ultrashort laser technology that characterizes, compensates, and modulates the femtosecond laser pulses using the SLM. MIIPS can not only measure the pulse, but also correct the high-order dispersion. Other means, such as FROG (frequency resolved optical gating) and SPIDER (self-referencing spectral phase interferometry for direct electric reconstruction) have been developed, but these can only measure the pulse characteristics and do not correct for defects. The MIIPS method is based on optical feedback from second-harmonic generation (SHG) in a non-linear crystal. A pulse shaper is used to apply a varying GDD to the pulse. The intensity of the SHG signal is at a maximum when the outgoing pulse is un-chirped, which occurs when the applied GDD exactly compensates the incoming pulse GDD. That is, when the pulse phase is equal to the phase correction. By spectrally resolving the SHG signal, GDD can be measured as a function of frequency, so that the spectral phase can be measured and dispersion can be compensated to all orders [3]. Grating-coupling the incident light to the Au tip also introduces a change in relative phase. The MIIPS process can also be used to shape the pulse to compensate the relative phase change introduced from the grating-coupling by maximizing the signal emitted at the tip apex, which is described further in Section 4.2.

The un-chirped, pulsed broadband laser light first goes through a 780 nm long-pass filter. So, the excitation spectrum only includes wavelengths longer than 780 nm, as shown in Figure 8. The incident light is then grating-coupled into SPPs that propagate toward the apex, adiabatically compress with accompanying field enhancement, and generate a nonlinear optical response predominantly in the nanoscopic apex volume, as previously described. The signal emitting at the tip apex is mostly the fundamental excitation signal. That is, the incident broadband light couples into a broadband SPP, then it is mostly emitted at the apex as light with the same spectrum as the incident light. There is only a small amount of nonlinear optical response. In order to measure this nonlinear optical response, in this case the FWM and HEL, the optical emission at the apex is directed through a 780 nm short-pass filter. Because the fundamental spectrum (same as the excitation spectrum) only has wavelengths greater than 780 nm, the fundamental signal

is completely filtered out. The signal that passes through the short-pass filter is only that from the nonlinear optical response, sharply cut off at 780 nm. This signal is then measured using a spectrometer (f =500 mm, SpectraPro 500i, Princeton Instruments).

4.2 Measurement Protocol

The protocol for measuring the FWM and/or HEL signal at the apex of a Au nanoantenna is sparsely documented. This subsection will describe how to measure the signals and how to approach the tip to a sample, which will be a useful reference for future Raschke group members.

The tuning fork, with the tip mounted, is placed in a custom-built holder, and a screw is used to tighten the tuning fork leads in place. Each leg of the tuning fork is connected to a BNC cable that connects to an R9 Control System (RHK Technology). The tip needs to first be roughly aligned to intersect with the beam path. A lamp is used to illuminate the tip, and the photodiode (PD) is used to observe the tip position on a TV screen. The M21 mirror is flipped down so light from the side of the tip is directed to the photodiode. The objective lens L1 gives a "far" view of the tip, and large adjustments are made to the position of the custom-built holder until the tip is visible at the photodiode, meaning the tip is roughly in the beam path. The M21 mirror is then flipped up so light from the tip apex is directed to the photodiode. The objective lens L2 gives a "close" view of the tip, and small adjustments are made to the position of the custom-built holder until the tip apex is visible at the photodiode, meaning the tip is aligned in the beam path. The lamp is then turned off.

Next, the Ti:Sa laser is turned on, and the oscillator system must be mode locked. The pulsed light is sent through the SLM, then it is directed through a neutral density (ND) filter to the sample box. The ND filter makes sure that the full power of the laser does not damage the tip apex, and it allows the fundamental signal at the apex to be weak enough to detect at the spectrometer without additional filters. The light is directed

onto the grating of the tip after L1. Piezoelectric actuators attached to M17 and M16 are used to change the position of the incident laser beam to hit the grating. When the position of the incident beam is maximal for grating-coupling, a bright spot is visible at apex of the tip. This is from the SPP emitting as a photon at the tip apex. An image of the tip apex with a bright spot, as seen at the photodiode through the "close" view (via L2), is shown in Figure 9. In between L3 and L4, the light is focused to a point,

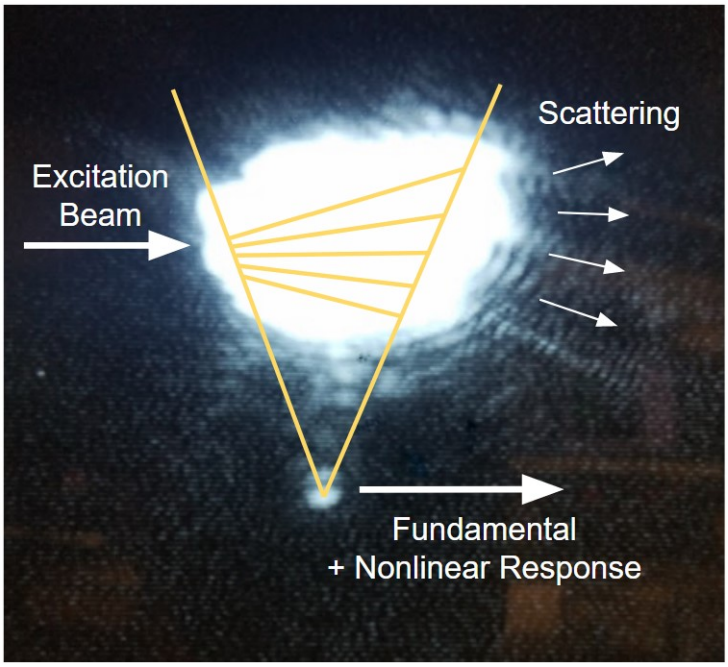

Figure 9: Image of the tip apex, as seen at the photodiode through the "close" view (via L2). Notice the incident light scattering at the grating (top), the region where there is no optical emission between the grating and the apex, and the bright spot where the signal is re-emitted at the apex (bottom). The yellow lines are to reference the location of the tip and grating. The excitation beam hits the grating structure, causing some scattering to emit, and the fundamental signal and nonlinear response emits at the tip apex. Figure created by author.

and a 50 µm pinhole is added to block out all of the excess scattering light and only transmit the light at the tip apex. The light at the apex is then sent to a spectrometer (Princeton Instruments Acton SpectraPro SP-2500 with ProEM 1600^2 Spectrometer). The piezoelectric actuators are used to adjust the position and focus of the incident laser light until the signal at the apex, which is mostly the fundamental spectrum, is at a maximum, which occurs when the spectrum has the highest intensity. The region of interest (ROI) for the spectrometer is also adjusted to maximize the spectrum intensity.

Finally, the short-pass filter is added before the spectrometer, and the ND filters are adjusted such that the laser power is ∼10 mW at the grating. Now, only the nonlinear optical response reaches the spectrometer, as all of the fundamental signal is filtered out.

A specialized LabVIEW program is run to reset and calibrate the spatial light modulator (SLM). Then, another program is used to apply a group delay dispersion (GDD) that exactly compensates the incoming pulse GDD to remove the chirp from the laser pulse. The exact GDD compensation is determined separately before this experiment, and the compensation file is saved for future use, but it must be created every few months as the laser spectrum destabilizes with time. Finally, a LabVIEW program is used to find a GDD compensation that counters the relative phase change induced by the light coupling to grated surface of the tip. Essentially, different GDDs are applied across a range of 600 fs^2, and the intensity of the nonlinear optical response at the tip apex is recorded. The intensity of the signal is strongest for the applied GDD that compensates for the phase change introduced by the grating-coupling process. An example of this GDD scan is seen in Figure 10. A file is created that applies this particular GDD compensation, and it is applied to the pulse for the rest of the experiment.

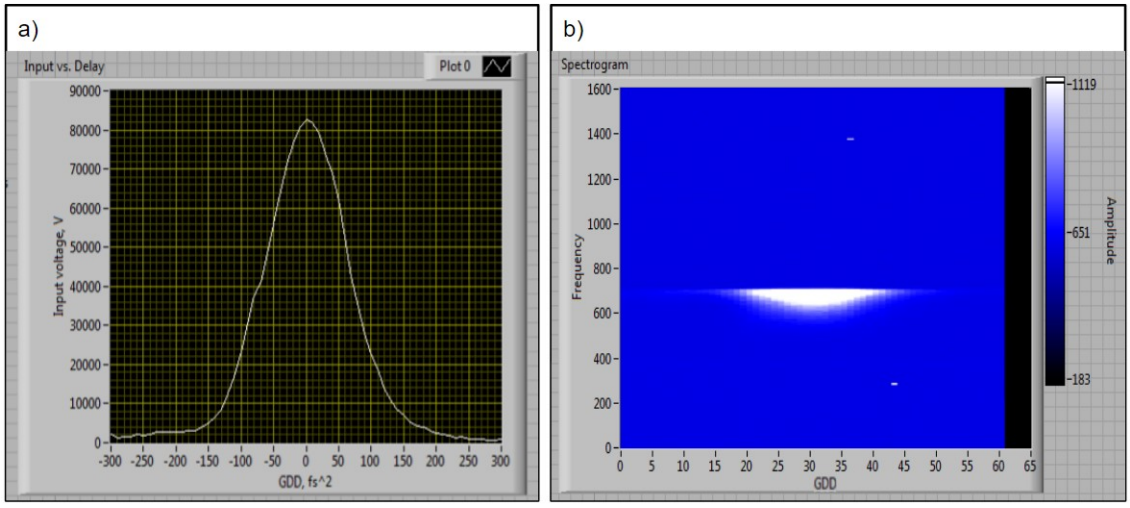

Figure 10: Example of a GDD scan. This is done after a particular compensation is applied, then a 600 fs^2 range around that GDD is applied to find where the intensity of the signal is the strongest. a) Plot of the intensity of the signal as a function of different applied GDDs, showing a peak intensity at the previously applied compensation. b) Spectrograph that shows the spectrum of the signal at the tip apex in the yz plane as a function of the GDD. Figure created by author.

At this point, the nonlinear optical response of the Au nanoantenna, including the FWM and sometimes the HEL, is measurable at the tip apex. We can use the spectrometer to measure the spectra of these signals for a tip that is far away from a sample ("free-standing" tip). Experimental results and analysis from measuring the FWM and HEL for a free-standing tip are included in Section 5.1.

In order to study the FWM and HEL signal in a variable nanoscale separation as described in Section 2.6, the tip must approach a flat Au sample with subnanometer resolution. This distance control is achieved through shear-force AFM using the R9 Control System (RHK Technology), similar to previous studies of this coupling regime [4]. First, a sample is prepared with a thin, flat layer of Au on a $\sim$1 cm square wafer of silicon. The sample is adhered to a magnetic sample disk, and the sample is placed under the tip apex on a magnetic base. Next, a "frequency sweep" is performed for the tip on the tuning fork. Essentially, when a voltage is applied to the tuning fork, it will vibrate at a certain frequency. A frequency sweep is performed to find the resonant frequency where the oscillations are stable with time, the amplitude of the oscillation is reasonable, and the Q factor is high. From previous experiments with these tips and tuning forks, the center frequency tends to be between 29 - 30.9 kHz, the nominal amplitude is $\sim$1 V, and the Q factor is on the order of 10^3. It is important to note that the tip/tuning fork is likely to shift during experimentation. If the tip shifts during the experiment, it will either crash into the sample or move to an unknown position. To minimize the risk of the tip shifting, the tip is kept in the system oscillating at the determined center frequency for at least 12 hours. The stability of the tip oscillation frequency can be tracked over long periods of time by measuring the "dF" parameter in the R9 Control System to see if the tip is stable.

Using a piezoelectric actuator, the sample is brought close to the tip surface until both the tip apex and the flat sample can be seen at the photodiode from the "close" view (via the L2 beam path). The sample can then be brought closer to the sample using a finer resolution piezoelectric actuator that is controlled in the R9 controller software. The center frequency is manually adjusted so the "dF" parameter is 0 mHz, and then the

sample is allowed to approach the oscillating tip using the finest resolution piezoelectric actuator. When the tip experiences shear forces, the sample retracts, and the tip and sample are now "in contact". The details of this approach are beyond the scope of this thesis, but they are well-documented in the R9 Control System manual. With the tip "in contact", it is very close to the sample (roughly 10 - 100 nm). We can now approach the sample to the tip using the finest resolution actuators, which can move in $\sim$500 pm increments. Because the position relative to the sample is not known, while approaching the sample to the tip, the change in oscillation frequency (dF) and amplitude of oscillation is monitored. The details of this are in Section 4.3, but these parameters are used to determine when the tip is too close to the sample and needs to be retracted. As the tip gets closer to the surface, dF will increase, and the amplitude of oscillation will decrease. If the tip gets too close, it will crash into the sample, which ruins the tip apex. We can record the intensity of the nonlinear optical response at the apex while the sample approaches the tip, or we can use specialized programs to take full spectral measurements at a set exposure time at each increment of the approach. The increment step, the rate of approach, and the total approach length can all be set in the R9 Controller software. The results of this approach of the sample to the tip apex are included in Section 5.3.

4.3 Shear-Force Atomic Force Microscopy and Scanning Tunneling Microscopy

In order to study how nonlinear signals change at small gaps, it is essential to have precise control of the distance between particles. This control can be realized in many ways, including modern fabrication processes that are used to create structures with sub-nanometer detail. For nanoantenna-surface setups, as previously described, it is common to use a well-established microscopy method with extremely precise piezoelectric motors to establish control of the distance between the tip apex and the sample surface. Precise control of this distance allows researchers to create a variable separation between structures and study the plasmonic and optical phenomena in the presence and absence of

quantum tunneling effects, as mentioned in the previous section.

Shear-force AFM and STM are common microscopy methods that are used to achieve nanometer distance control when varying the gap between a Au nanoantenna and a Au substrate. Both methods are based on feedback loops using a measurable parameter that changes with the tip-substrate distance to determine how the piezoelectric motors should respond to keep a constant distance [4]. Both microscopy systems have well-established hardware and software that is commercially available from many companies like RHK, Attocube, and Bruker, so they can easily be used in experiments that require a variable tip-substrate distance.

The basic principle of the shear-force AFM system depends on detecting shear forces between the tip of a nanoantenna and the surface. A diagram of the operation is shown in Figure 11. The tip is attached to one leg of a small quartz tuning fork, which oscillates

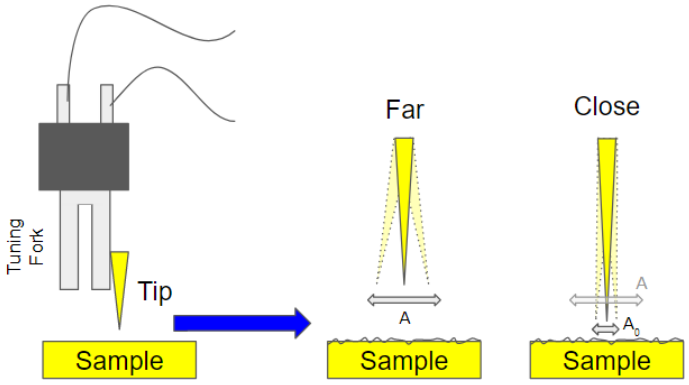

Figure 11: Basic diagrams of shear-force AFM. The left diagram shows how the tip is attached to a tuning fork. The middle diagram shows the oscillating tip amplitude at a far distance from the surface, and the right diagram shows the oscillating tip at a close distance. The amplitude of the tip oscillations for the far and close tip-surface distance is given by A and A_0. Figure created by author.

when a voltage is applied to it. The tip-tuning fork apparatus then approaches the surface using a piezoelectric motor, which is a type of motor that uses how piezoelectric metals change shape when an electric field is applied to create motion. When the tip is close to the surface and experiences shear forces, those forces dampen the tuning fork oscillations, so the amplitude of oscillation decreases from A to A_0. The change in electric oscillations in the quartz leads to a voltage response, which is read as an output. If the tip moves

closer or farther from the surface due to external forces or vibrations, that movement is realized as a change in the voltage response, so the piezoelectric motor controller can adjust accordingly to maintain a constant distance with subnanometer resolution [11]. So, the voltage response from the presence of shear-forces between the tip and the surface is used as feedback for a computer to know how much to adjust the piezoelectric motor to maintain a constant gap size.

The basic operation of an STM starts by applying a bias voltage between the conducting tip and the conducting substrate. A diagram of an STM system is shown in Figure 12. For small distances between the tip and the substrate, electrons can tunnel through

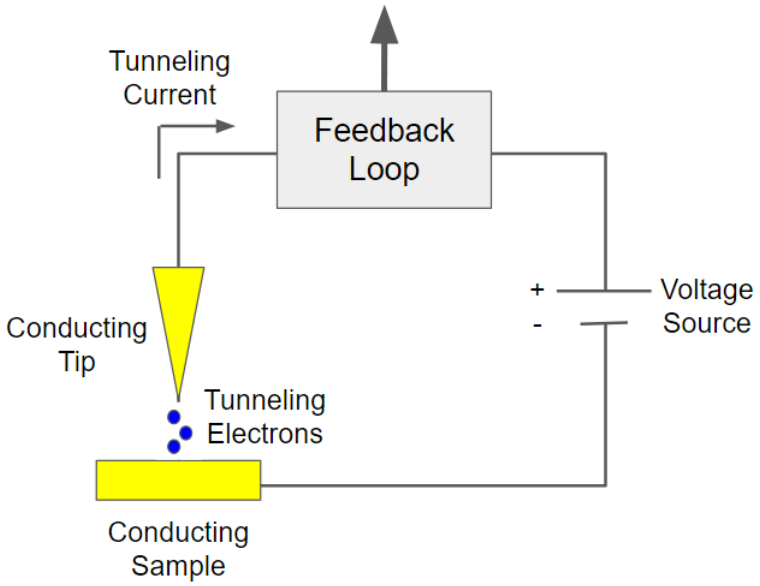

Figure 12: Diagram showing the basic operation of STM. Figure created by author.

the gap, creating a tunneling current. In brief, the ability for an electron to quantum tunnel is a result of small particles having prominent wave-like properties. Objects can be described using a wave function that gives the relative probability of that object being at any position. Of course, the object is nearly certain to be at a single, obvious position. However, for small objects like electrons, the spatial distribution of the wave function turns out to give a considerable nonzero probability that an electron previously on one end of a gap is suddenly on the other end of the gap. The number of electrons that tunnel increases as the size of the gap decreases because the probability of an electron

tunneling across a smaller distance is greater than the probability of an electron tunneling across a larger distance. So, the tunneling current increases when the tip-surface distance decreases. That tunneling current is measured as the output of the system, so if the tip moves closer or farther from the surface due to external forces or vibrations, the change in tunneling current is realized by an ammeter, and the piezoelectric motor adjusts the tip distance to keep gap size constant.

STM is particularly useful for studying how optical mechanisms change in the quantum tunneling regime, but it is worth noting that the introduction of light-matter interactions to the tip-surface apparatus introduces new sources of current that need to be considered. An STM is a great tool when investigating nonlinear optics in the quantum tunneling regime because when the tip approaches the Au sample, the presence of any tunneling current indicates that the tip and the sample are in a tunneling regime [4]. However, when the nanoantenna is illuminated with laser light, the tunneling current measured in the STM setup is actually a sum of the static tunneling current from the bias voltage and an additional photoinduced current from the incident light. This additional current is from the transfer of excited electrons from the incident laser light across the gap. This transfer can occur either if enough photons excite the electron to give it enough energy to exceed the barrier between the tip and the substrate, or if the excited electron does not have the energy to exceed the barrier, but experiences photoassisted tunneling. Either way, it is necessary to consider that the STM current for an illuminated nanoantenna still depends on the tip-surface distance, but the dependence is now a function of both the bias voltage and the power and spectrum of the incident laser [21]. Both shear-force AFM and STM are effective methods for approaching a nanoantenna to a flat surface, and these technologies enable researchers to investigate nonlinear light-matter interactions in new regimes with incredible spatial precision.

4.4 Implementing a Scanning Tunneling Microscope

Previously, the experimental setup we use in this study did not have a scanning tunneling microscope. While experiments have been done with this setup using STM interaction, combining STM interaction with nanometer distance control and femtosecond laser science is not an easy task. Further, most of the previous experience with STM in this experiment is not well documented and was long lost. To introduce a functional STM to the system, extensive testing was completed. While the STM component of this experiment is still being designed, a number of tests and designs have been successful, which are included in Section 5.4.

Creating a bias voltage between the tip and the sample with the R9 Control System requires a two-step preamplification process. Each step of the preamplifier converts a weak electrical signal into an output signal strong enough to be noise-tolerant and useful for further processing. A second-stage R9 IVP Preamp is used to create a bias voltage, which is set in the R9 software, between two terminals (labeled "input" and "bias"). This second-stage preamp is a bias-preamp interface module that converts a differential bias output from the R9 into a single-ended bias signal the tip. It also converts the single-ended preamp signal from a first-stage preamplifier into a differential output signal that can be read by the R9 System. The bias terminal is connected directly to the sample. The input terminal is connected to a first-stage preamplifier (IVP-200), which is then connected to the tip. The output of the preamp is connected directly to the R9 system for processing and measurement. A schematic of the setup is shown in Figure 13.

It was necessary to make substantial modifications and tests to the existing R9 software to measure the tunneling current as a function of tip position. In addition to being able to measure the tunneling current, this modified program can use the tunneling current as a threshold for retracting the tip. Because the tunneling current consistently increases exponentially as the tip gets closer to the sample, the program can be modified to retract the tip when the tunneling current exceeds 9 nA, which was found to be approximately the tunneling current when the tip is one increment away from crashing into

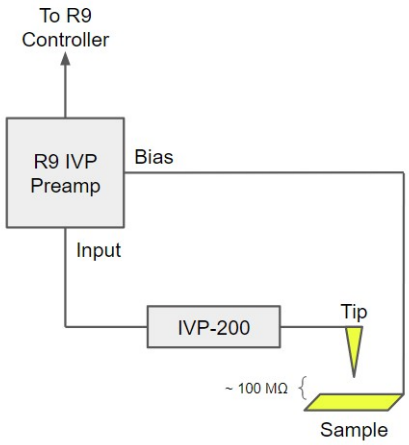

Figure 13: Schematic of the STM setup using an R9 System Controller. Figure created by author.

the surface. This threshold agrees with the results from previous studies, which shows that at ∼0 nm from the surface, there is ∼10 nA of tunneling current between the tip and the surface [4]. By using both a tunneling current threshold and a threshold for the change in oscillation frequency dF and amplitude (as used before), we can decrease the likelihood that the tip will accidentally crash into the surface.

For the first tests of the STM, one leg of the tuning fork, which is in electrical contact with the Au tip, is used to connect the tip to the preamplifier. However, it turns out that this approach results in inconsistent tunneling current measurements, which is discussed and solved in Section 5.4. For the flat Au sample to be connected to the preamplifier, we must connect the surface to a wire that can be connected to a BNC cable. This is done by using a two-part conductive silver epoxy to glue a gold wire to the surface of the sample, then using a BNC-to-hook cable to grab onto the gold wire. The Au sample with a connection for use in STM is shown in Figure 14. This approach also works for making other interesting samples to investigate using STM, such as graphene and WSe_2.

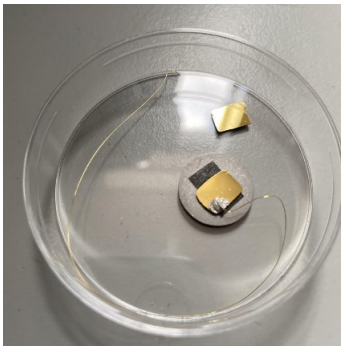

Figure 14: Picture of flat Au sample with a silver wire attached for use in an STM circuit. Figure created by author.

5 Measurements and Analysis

5.1 FWM and HEL Power Dependence

Using the protocol outlined in Section 4.2, the FWM and HEL signals at the apex of a free-standing tip (not near a flat Au sample) are measured for different excitation powers. A variable ND filter is used to filter the femtosecond-pulsed laser light before it grating-couples and excites the Au in the nanoantenna. The spectra of the FWM and HEL are measured with an excitation power of 6.57 mW, 7.46 mW, 8.49 mW, and 10.54 mW. The resulting spectra, measured with a 30 s exposure time, are shown in Figure 15.

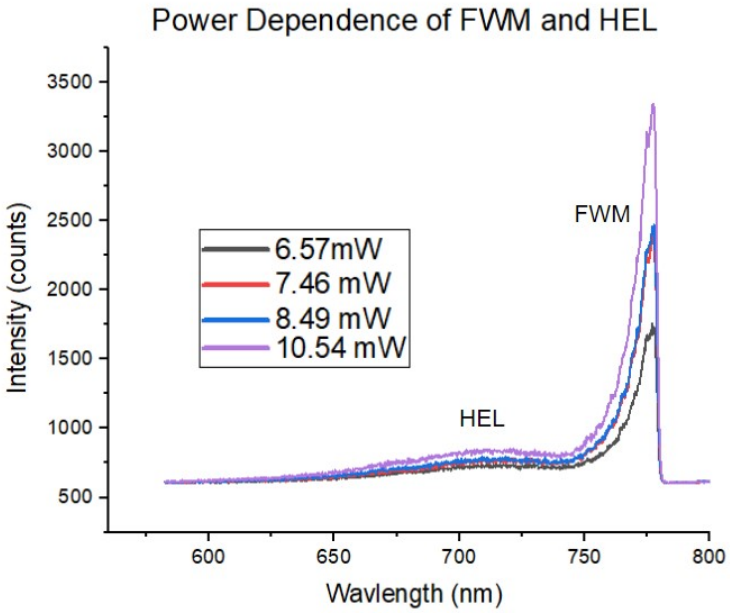

Figure 15: Plot of the FWM and HEL spectra for different excitation powers. Figure created by author.

5.2 Fitting the Data and Plasmon Lifetime

While the raw data is a good visual indication of a successful measurement, it is difficult to analyze and process raw data. It is much easier and useful to analyze and process continuous functions. Further, the FWM and the HEL signals are overlapping, so it is difficult to conclude what part of the raw spectrum is from each signal where they overlap. Following the methods of previous studies, we deconvolute the overlapping FWM and HEL spectra by fitting the total spectrum to a double-Voigt profile [22]. A Voigt profile is a distribution given by a convolution of a Gaussian distribution and a Cauchy-Lorentz distribution. It is basically a fit function that combines both a Gaussian and a Lorentzian distribution, and it is often used in analyzing data from spectroscopy. An example of the spectral fits, including the double-Voigt profile (blue line) and the deconvoluted HEL (orange line) and FWM (green line) spectra, is shown for 10.54 mW excitation power in Figure 16. It is worth noting that the spectral fitting of the FWM goes beyond the 780 nm (∼1.6 eV) cutoff. The FWM is not just a simple Voigt peak. As discussed previously, it is distinctly structured based on the electron transitions shown in Figure 1. However, it is a reasonable assumption to consider a peak at ∼1.5 eV when fitting the tail end of the spectrum, according to previous studies [22].

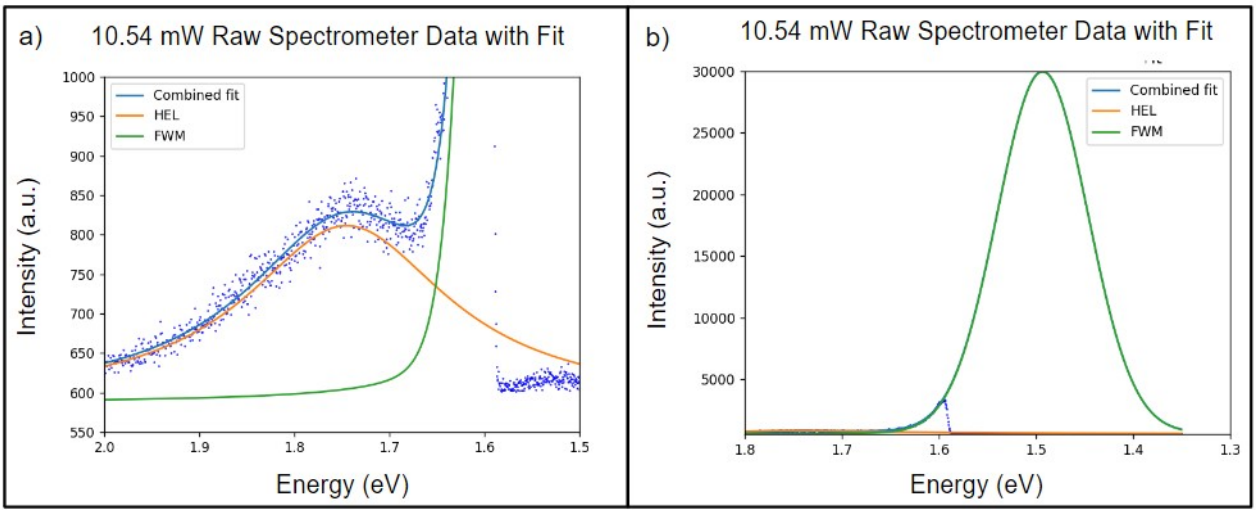

Figure 16: Example of raw spectrometer data with functional fits for 10.54 mW excitation power. The scale in a) focuses on the HEL spectrum and fit, and the scale in b) focuses on the FWM spectrum and fit. Figure created by author.

After obtaining a functional form of the spectra from this fitting technique, we can find the integrated intensity of the spectra. The integrated intensity of the spectra for each excitation power is shown in Figure 17. Using this fitting program, one could investigate various parameters of the spectra, such as the peak intensity, the peak position, the full width at half maximum (FWHM), and the line width. From the line width, we can calculate the plasmon lifetime following methods from previous studies, which can give an initial insight on the plasmon decay process [4]. The calculated lifetimes, τ, for the FWM and HEL at each excitation power is given in Table 1.

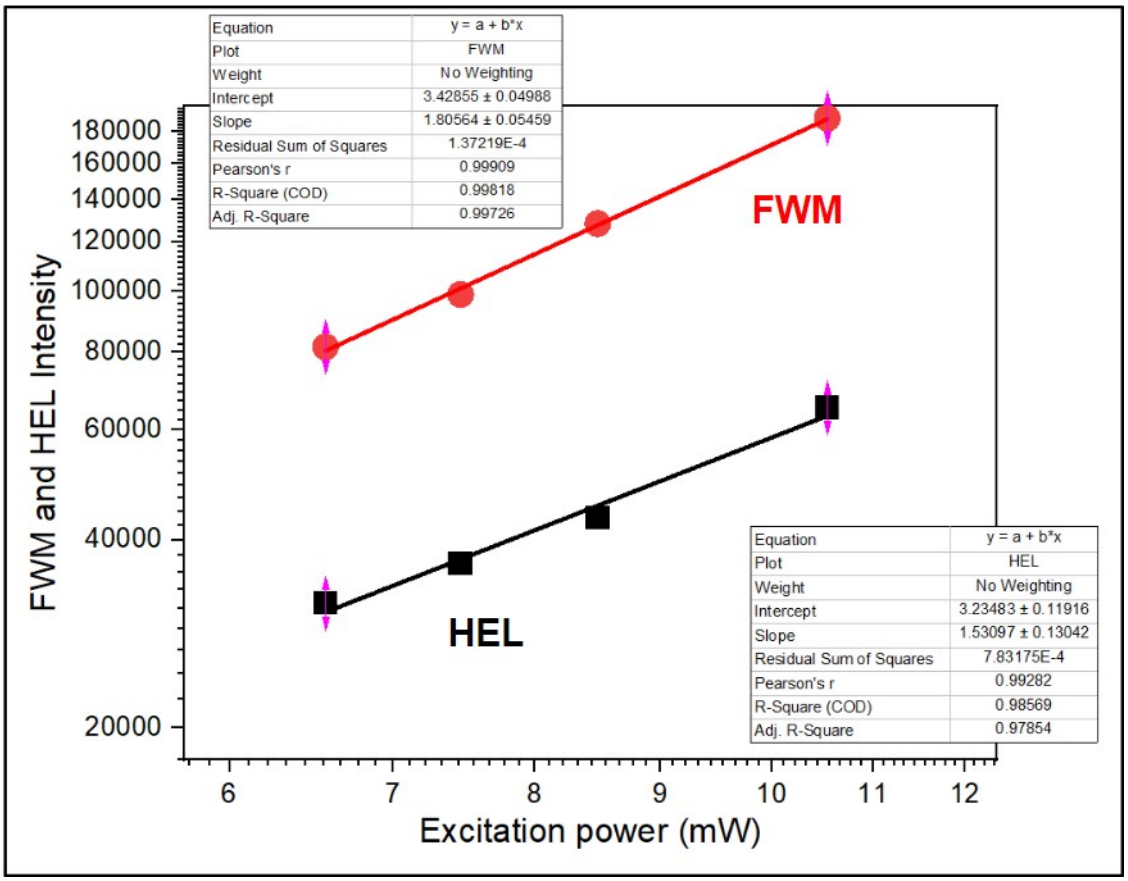

Figure 17: Power dependence of the integrated intensity of each spectrum from the functional fits. The red line is from the FWM, and the black line is from the HEL. The parameters for the line of best fit for each power dependence is displayed next to the line. Figure created by author.

Power	FWM Width [eV]	$\tau = \frac{2\hbar}{\Gamma}$ [fs]	HEL Width [eV]	$\tau = \frac{2\hbar}{\Gamma}$ [fs]
6.57 mW	0.0544	24.2	0.1174	11.2
7.46 mW	0.0547	24.1	0.1195	11.0
8.49 mW	0.0549	23.9	0.1193	11.0
10.54 mW	0.0546	24.1	0.1297	10.1

Table 1: Plasmon lifetimes calculated from linewidth of the FWM and HEL signal at each excitation power.

5.3 FWM Approach to Flat Au Sample

Unfortunately, the HEL signal is typically not visible at the tip apex. Exactly why is unclear, but despite success with increasing the tip quality, the HEL signal was only strong enough for measurements from a few tips out of the hundreds that were fabricated. Approaching the tip with a flat Au sample adds complexity and instability to the experiment, so we were not able to measure the HEL signal as a function of tip-sample distance as we intended. However, we more frequently measured a strong FWM signal from the nanoantenna apex. As a proof on concept, and to firmly establish the validity of the measurement protocol, the FWM signal was measured as a function of distance between the tip apex and the Au sample surface.

As a preliminary investigation, the FWM intensity was first measured directly using a pre-existing program that interfaces the spectrometer and the R9 Control System. This measurement, although it was noisy, showed the intensity of the FWM increase between a tip-sample distance of 10 nm to 2 nm and decrease between 2 nm and 0 nm. This result is nearly identical to the enhancement and quenching seen for a photoluminescent signal at the apex of a Au nanostructure in the motivational previous study [4]. Unfortunately, as is often the case for a close tip-sample approach, the tip crashed into a surface as a result of this measurement, and it could not be repeated with the same tip.

Using a new tip with a strong FWM signal at the apex, we approached the sample to the tip again and took full spectral measurements at each position of the approach. With measurements of the spectrum at each distance, we are able to use the previously

described fitting program to investigate various parameters of the FWM spectrum, such as the integrated intensity, the peak position, the full width at half maximum (FWHM) as a function of distance between the tip apex and the sample. Although we do not have data showing the FWM and the HEL signal as a function of tip-sample distance, the program is still capable of deconvoluting an overlapping FWM and HEL spectra and plotting the separated spectra as a function of distance. Figure 18 shows an example of the raw spectral data of the FWM signal as a function of tip-sample distance, as well as the fit spectra.

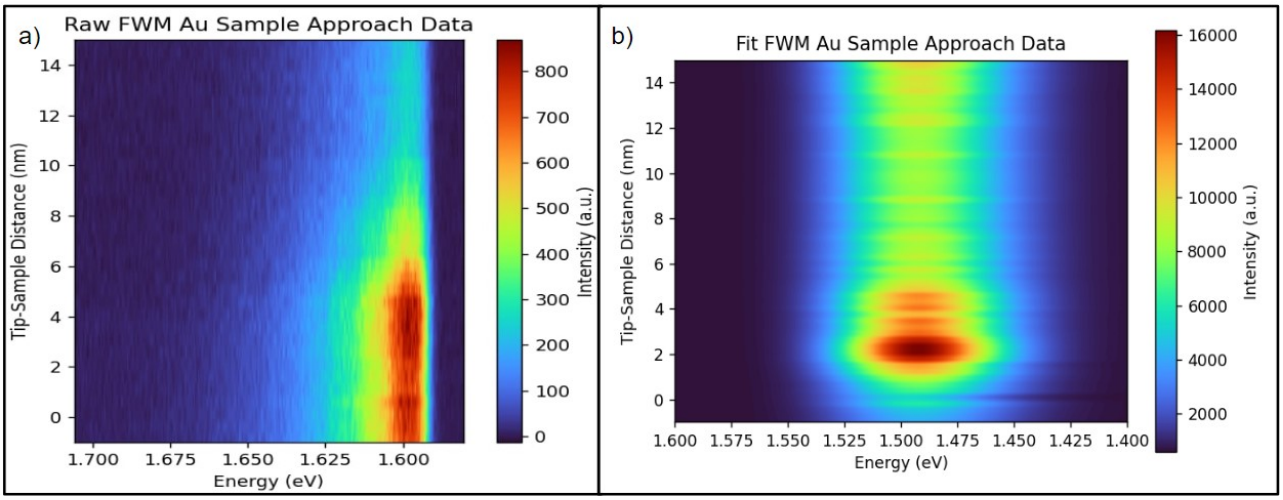

Figure 18: Example of a) raw spectral data and b) functional fits for the FWM during an approach of the tip apex to the flat Au sample surface. Figure created by author.

5.4 STM Successes

Although many challenges were faced when building the STM part of this experiment, there were a number of successful milestones. As mentioned before, we now have a program that will retract the tip from the sample when a tunneling current threshold is reached, which in combination with the dF and amplitude threshold, we can decrease the likelihood that the tip will accidentally crash into the surface during a measurement. We performed many successful approaches of the tip to the sample surface and measured the tunneling current. An example of the tunneling current for successful STM approaches

is shown in Figure 19. This result shows a consistent tunneling current increase during the approach across three trials. Further, the tunneling current begins to increase when the tip is ∼3 nm from the surface and increases roughly exponentially, which is consistent with previous measurements [4].

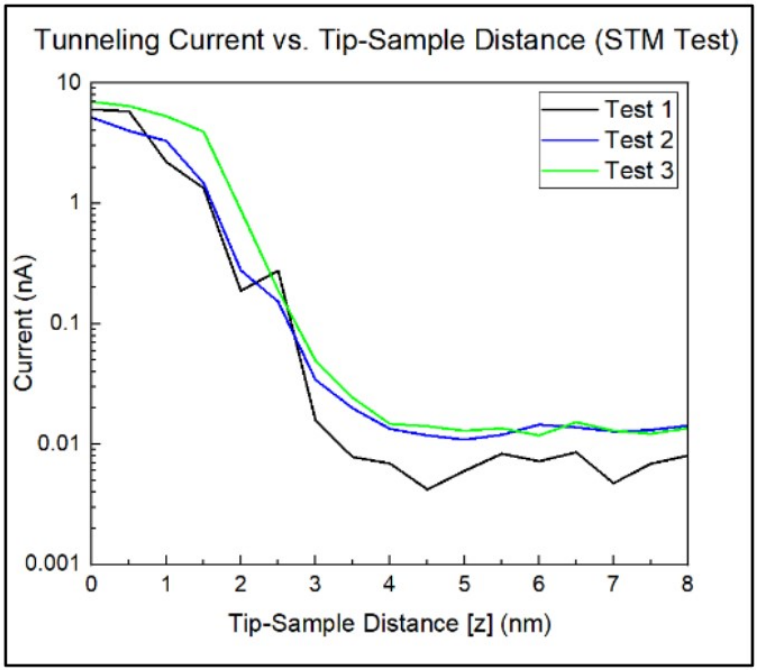

Figure 19: Tunneling current as a function of tip-sample distance, showing a consistent tunneling current increase that agrees with previous studies. Figure created by author.

However, when we tried to measure the tunneling current in parallel with the optical signal at the tip apex during an approach, we realized that the tunneling current measurement was often inconsistent and noisy. The tunneling current sometimes increases slower then expected, and sometimes starts to increase before or after the expected 3 nm distance. Further, there is an unknown background current, which is subtracted from Figure 19, but may be relevant to the current inconsistencies. We determined that the inconsistencies and background current is a result of cross-talk between the amplifier that is used to drive the tuning fork oscillation and the STM circuit. This is a result of measuring the STM current through the same leg of the tuning fork that is used to drive the oscillation of the tuning fork. Various alternative connection schemes were attempted with no success at eliminating this cross-talk while still being able to make a stable approach. So, we eliminated the source of inconsistency by electrically isolating the Au tip

from the tuning fork and connecting the tip to the STM circuit via a separate 0.127 mm silver wire. A diagram of the new tip design is shown in Figure 20.

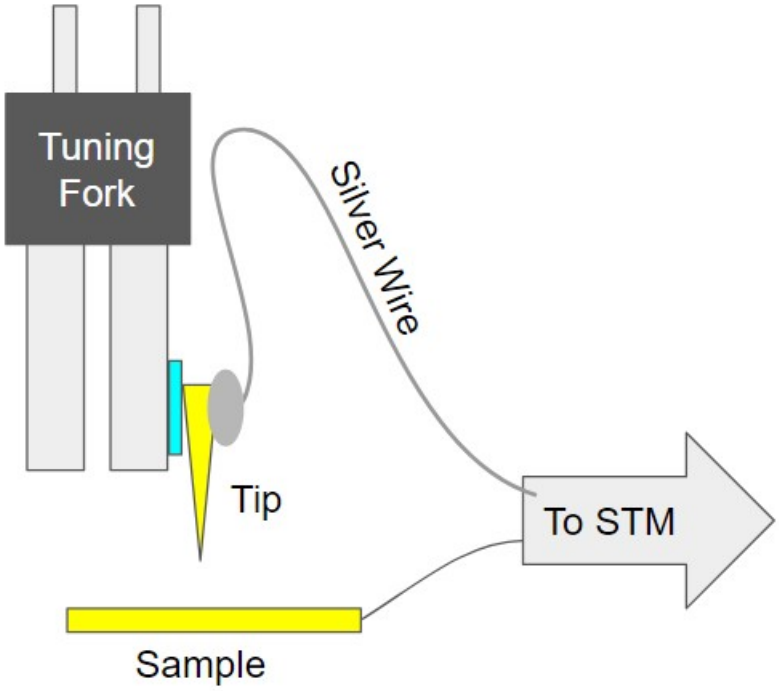

Figure 20: Diagram of STM tip design. The cyan rectangle is optical glue that electrically separates the tuning fork from the tip. Figure created by author.

With this new tip design, the silver wire needs to be connected using a silver epoxy before the grating is added to the tip using the focused ion beam (FIB). This is because the tip needs to be connected to ground via the silver wire during the FIB milling process so that the charges from the ion beam do not build up on the tip. As mentioned before, charge build up during the FIB milling would cause a dull grating structure and consequent poor grating-coupling. It is also important to note that the added weight of the silver wire can effect the stability of the tip oscillation, which is essential to make an approach without crashing the tip into the surface. To avoid this instability, we attach the silver wire to the tuning fork mount close to the base of the tuning fork, which reduces the affect of the excess wire. Adding the silver wire to the tip takes a lot of production time and a delicate hand, but through trial and error, we created a procedure that can reliably make these tips with an STM connection. In brief, we build the STM tip under a 3x optical microscope. The silver wire is placed parallel and next to the tuning fork,

then it is bent at 90 degrees so the wire is in contact with and perpendicular to the Au tip. A slight hook is bent at the end of the wire away from the viewer so the wire hooks onto the Au tip. Silver epoxy is then added using a thin wire tool to glue the tip to the silver wire. An image of the finished product is shown in Figure 21. Each tip is tested using a multimeter to make sure that the tip is electrically isolated from the tuning fork and in electrical contact with the silver wire. Finally, when the STM tip is installed into the experiment, the silver wire is bent down and taped to the tuning fork holder, as shown in Figure 21. It is important that the silver wire is parallel to the tuning fork and has a little bit of slack before it is taped down, otherwise the excess weight/forces will negatively affect the tip oscillation stability. Although not as good as a tip without the silver wire, based on measurements of the Q factor and amplitude of the tuning fork oscillation, this design results in a tip oscillation that is still stable enough to make an approach. Unfortunately, we have not made an approach, but this design is the best option, and it will be used in future STM experiments with this experimental setup.

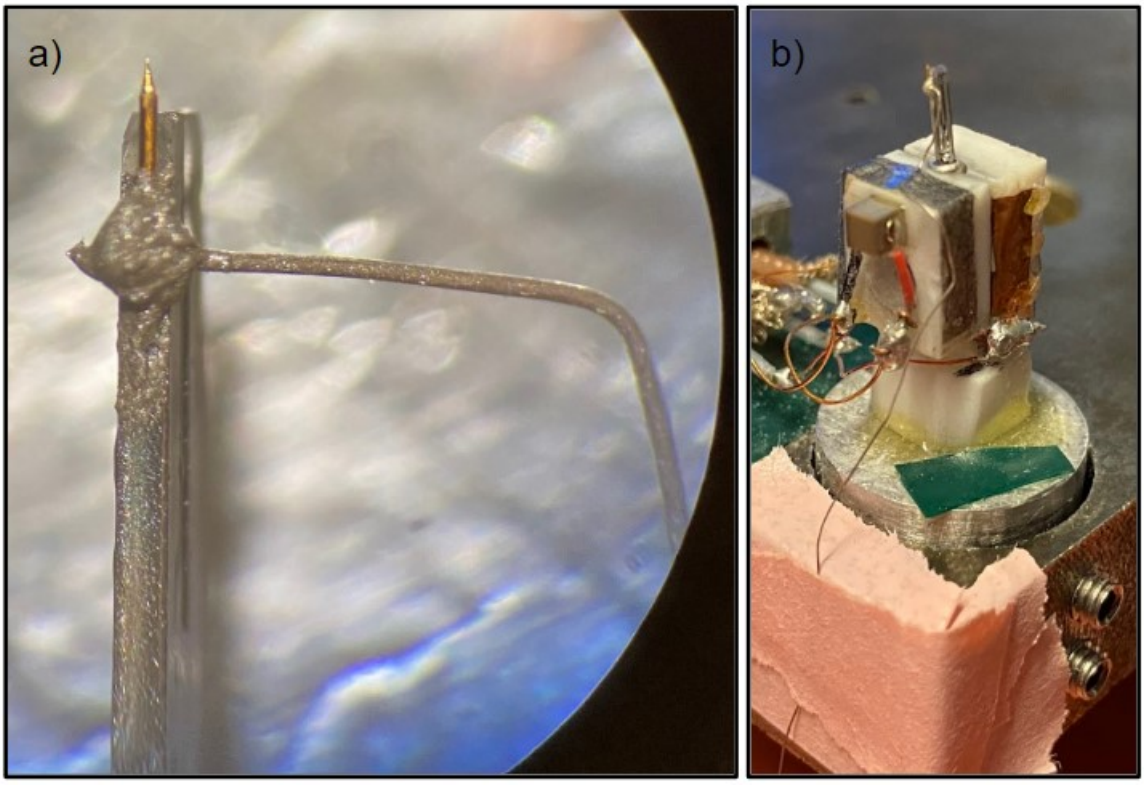

Figure 21: a) Image of STM tip on a tuning fork after the silver wire is glued on using silver epoxy. b) Image of STM tip fully installed in the tuning fork holder with the excess wire bent down and attached to the based of the holder. Image created by author.

6 Discussion and Conclusion

A few interesting conclusions can be made as a result of the preliminary measurements. From analysis of the linewidth of the spectra, we concluded a plasmon lifetime for the FWM signal of ∼24.1 fs and a plasmon lifetime for the HEL signal of ∼10.8 fs. Based on these calculations from the fit data and previous studies on emitter lifetimes, we tentatively conclude that the FWM signal lifetime corresponds to Drude relaxation, and the HEL lifetime corresponds to radiative damping [4]. However, the results are not yet corroborated, and more analysis of the existing data sets and repeated measurements are necessary to support this result. The power dependent measurements of the spectra are useful for developing a power law for the signal, which reveals the order of the signal (i.e. how many photons cause the excitation before the electron relaxes). The FWM and HEL for Au nanoantennas is already reported to be of 3rd and 2nd order, respectively [2]. However, the slope of the power dependence lines in Figure 17 are 1.8 for the FWM and 1.5 for the HEL. This result is inconsistent with previous studies, so further power dependent measurements of the HEL and FWM signals are necessary to make any sound conclusions. A final noteworthy observation from these experiments is from the measurement of the FWM signal during an approach of a flat Au sample to the nanoantenna. As shown in Figure 18, it was observed that the FWM signal increased from a tip-sample distance of ∼10 nm to ∼2 nm and started to decrease from ∼2 nm to 0 nm. This result is very exciting because in a previous study of photoluminescence from simply illuminating the tip apex (no grating-coupling or nanofocusing), it was found that the photoluminescent signal was enhanced from ∼15 nm to ∼2 nm and quenched from ∼2 nm to 0 nm [4]. The observation that the FWM signal is enhanced and quenched in the same regions as the photoluminescent signal is a strong indicatation of similar physical properties occuring, which warrants further investigation and repeated measurements to support this result.

As was observed during this project, these measurements using femtosecond laser science with nanometer distance control are not trivial. There are countless factors, such as tip quality, oscillation stability, external vibrations, complicated electronics, and

complicated processing code that all can result in failure to make a measurement or failure to detect a signal at all. The first step in making significant scientific discoveries is to get the experiment to work, and to get it to work consistently. A strong technical understanding of the physics and the experiment, as well as numerous tests and clever modifications are all necessary to achieve this goal.

The present work provides the necessary tools to further investigate the open science questions provided in the introduction of this thesis. The open science questions were "how does the FWM and HEL signal from a Au nanoantenna vary as a function of incident laser power, and what can we conclude about the plasmon lifetime?", "how does the FWM and HEL signal from a Au nanoantenna vary as we approach a Au sample?", and "how is the HEL and FWM signal quenched when we get into the tunneling regime, and how does the tunneling current correlate with the FWM/HEL signals?". To start, the tip fabrication process was dramatically improved. As a result, more tips will be usable in these types of experiments that address questions about the FWM and HEL signal in a Au nanostructure and during an approach to a flat Au surface. This will save researchers a considerable amount of time and money. The tip fabrication process and improvements discovered from making hundred of tips is now well-documented for future use. The general measurement protocol to measure the FWM and HEL signal in a Au nanostructure is also now, for the first time, documented and described in detail.

Significant progress was made in implementing a scanning tunneling microscope in the shear-force AFM setup, allowing future experiments to measure tunneling current in parallel with an optical signal. We not only successfully measured tunneling current during an approach, but we also modified the program procedure to use the tunneling current as a threshold for retracting the tip from the sample surface. This modification will decrease the likelihood of a tip crashing into the surface, allowing for future experiments with scanning tunneling microscopy to proceed with less risk of ruining the experiment. Although the tunneling current is still facing some inconsistencies, we have developed a procedure for making tips for the STM circuit, and we developed a design that limits cross-talk and minimizes the impact on tip oscillation stability. The next step

to further minimize the instability introduced by the added mass from the STM connection is to connect a thinner gold wire instead of a silver wire to the nanoantenna. For example, a 0.05 mm diameter gold wire will not only cut the weight in half, but gold is softer than silver, so the rigidity of the wire will impact the oscillations less. Successfully implementing an STM into the experiment allows us to correlate a tunneling current with the quenching of an optical signal in future experiments, contributing to answering the open science questions.

Finally, we now have code that successfully fits the raw data, making it more useful for analysis. We already were able to make a few tentative conclusions about the plasmon lifetime from analysis of the fit data. Future investigations of the FWM and HEL signal will require similar fitting, and the code is fully capable of deconvoluting the overlapping signals, allowing for separate analysis of each spectra. This will undoubtedly be used for a successful measurement of the FWM and HEL signal at the tip apex during an approach to a flat Au surface. In addition to establishing these critical tools for future investigations, we developed the physical framework and background necessary to understand experiments investigating the FWM and HEL response in Au nanostructures. This background review will serve as an excellent starting point for future investigations.

The limiting factor in answering the open questions is data, but the necessary tools are now well-established. Given a good enough tip with the perfect external conditions to allow for a stable approach, or further developments to make these measurements consistently, we will measure the FWM and HEL response of a Au nanoantenna during an approach in parallel with a tunneling current. In turn, this will open the floodgates to new scientific conclusions about the mechanisms at play. In general, the implementation of an STM system is relevant to future research projects on optically interesting 2D materials, such as graphene or transition-metal dichalcogenides (TMDs) like WSe_2. Future experiments could study how the enhancement and quenching of nonlinear signals in Au nanoantennas and corresponding tunneling current change when a 2D material is introduced between the nanoantenna and a metallic substrate, as 2D materials are relevant in many modern nanotechnologies.

The ability to control tip-surface distances with AFM and STM, use STM to indicate when the tip-surface distance is within the tunneling regime, and use SPPs to enhance previously difficult to detect nonlinear signals like the FWM and HEL suggest further experiments could be done to explore the unique optical properties of these nonlinear signals at the transition from the classical coupling regime to the quantum tunneling regime. Such future investigations could extend upon our preliminary result on how the FWM signal from a Au nanoantenna is optically quenched in the quantum regime and correlate the signals with a tunneling current between the tip and the surface. A tunneling current correlation with HEL could further solidify the debated emission mechanism and plasmon dynamics.

There are many applications of nonlinear signals in optical information processing that could result from this field of study. Using metallic nanostructures to create nonlinear signals is a critical step in merging optics and electronics, and research in the physics of these nanoscale light-matter interactions will certainly be a necessary part of the future development of advanced photonic circuits. Future electronics that use these principles of light-matter interactions will allow researchers and engineers to develop new switching and transistor models and allow electronics to realize faster processing speeds. The emerging studies on nonlinear signals at small separations give scientists and engineers a better understanding of how light and matter interact differently on scales where quantum effects are relevant, which will contribute to the development of future nanotechnologies and nanospectroscopy methods [1]. The development of technologies that utilize optical nonlinearties from metallic nanostructures will require scientists to continue to explore the challenging physical questions in this realm and broaden the collective understanding of light-matter interactions on a nanoscale.

7 References

[1] P. Dombi, Z. Pápa, J. Vogelsang, S. V. Yalunin, M. Sivis, G. Herink, S. Schäfer, P. Groß, C. Ropers, and C. Lienau, *Strong-Field Nano-Optics*, Rev. Mod. Phys. **92**, 025003 (2020). https://doi.org/10.1103/RevModPhys.92.025003.

[2] V. Kravtsov, S. AlMutairi, R. Ulbricht, A. R. Kutayiah, A. Belyanin, and M. B. Raschke, *Enhanced Third-Order Optical Nonlinearity Driven by Surface-Plasmon Field Gradients*, Phys. Rev. Lett. **120**, 203903 (2018). https://doi.org/10.1103/PhysRevLett.120.203903.

[3] V. Kravtsov, R. Ulbricht, J. M. Atkin, and M. B. Raschke, *Plasmonic Nanofocused Four-Wave Mixing for Femtosecond near-Field Imaging*, Nat. Nanotechnol. **11**, 459 (2016). https://doi.org/10.1038/nnano.2015.336.

[4] V. Kravtsov, S. Berweger, J. M. Atkin, and M. B. Raschke, *Control of Plasmon Emission and Dynamics at the Transition from Classical to Quantum Coupling*, Nano Lett. **14**, 5270 (2014). https://doi.org/10.1021/nl502297t.

[5] S. Berweger, J. M. Atkin, X. G. Xu, R. L. Olmon, and M. B. Raschke, *Femtosecond Nanofocusing with Full Optical Waveform Control*, Nano Lett. **11**, 4309 (2011). https://doi.org/10.1021/nl2023299.

[6] P. A. D. Gonçalves, N. Stenger, J. D. Cox, N. A. Mortensen, and S. Xiao, *Strong Light–Matter Interactions Enabled by Polaritons in Atomically Thin Materials*, Adv. Opt. Mater. **8**, 1901473 (2020). https://doi.org/10.1002/adom.201901473.

[7] A. Manjavacas, J. G. Liu, V. Kulkarni, and P. Nordlander, *Plasmon-Induced Hot Carriers in Metallic Nanoparticles*, ACS Nano **8**, 7630 (2014). https://doi.org/10.1021/nn502445f.

[8] A. Giugni, B. Torre, A. Toma, M. Francardi, M. Malerba, A. Alabastri, R. Proietti Zaccaria, M. I. Stockman, and E. Di Fabrizio, *Hot-Electron Nanoscopy Using Adiabatic Compression of Surface Plasmons*, Nat. Nanotechnol. **8**, 845 (2013). https://doi.org/10.1038/nnano.2013.207.

[9] M. Garg and K. Kern, *Attosecond Coherent Manipulation of Electrons in Tunneling Microscopy*, Science **367**, 411 (2020). https://doi.org/10.1126/science.aaz1098.

[10] X. Wang, K. Braun, D. Zhang, H. Peisert, H. Adler, T. Chassé, and A. J. Meixner, *Enhancement of Radiative Plasmon Decay by Hot Electron Tunneling*, ACS Nano **9**, 8176 (2015). https://doi.org/10.1021/acsnano.5b02361.

[11] E. Betzig, P. L. Finn, and J. S. Weiner, *Combined Shear Force and Near-field Scanning Optical Microscopy*, Appl. Phys. Lett. **60**, 2484 (1992). https://doi.org/10.1063/1.106940.

[12] C. Tang, Z. He, W. Chen, S. Jia, J. Lou, and D. V. Voronine, *Quantum Plasmonic Hot-Electron Injection in Lateral $WSe_2/MoSe_2$ Heterostructures*, Phys. Rev. B **98**, 041402 (2018). https://doi.org/10.1103/PhysRevB.98.041402.

[13] O. Lozan, R. Sundararaman, B. Ea-Kim, J.-M. Rampnoux, P. Narang, S. Dilhaire, and P. Lalanne, *Increased Rise Time of Electron Temperature during Adiabatic Plasmon Focusing*, Nat. Commun. **8**, 1656 (2017). https://doi.org/10.1038/s41467-017-01802-y.

[14] T. Haug, P. Klemm, S. Bange, and J. M. Lupton, *Hot-Electron Intraband Luminescence from Single Hot Spots in Noble-Metal Nanoparticle Films*, Phys. Rev. Lett. **115**, 067403 (2015). https://doi.org/10.1103/PhysRevLett.115.067403.

[15] Y. Liu, Q. Chen, D. A. Cullen, Z. Xie, and T. Lian, *Efficient Hot Electron Transfer from Small Au Nanoparticles*, Nano Lett. **20**, 4322 (2020). https://doi.org/10.1021/acs.nanolett.0c01050.

[16] F. Vázquez, D. Kobayashi, I. Kobayashi, Y. Miyamoto, K. Furuya, T. Maruyama, M. Watanabe, and M. Asada, *Detection of Hot Electron Current with Scanning Hot Electron Microscopy*, Appl. Phys. Lett. **69**, 2196 (1996). https://doi.org/10.1063/1.117163.

[17] S. R.-K. Rodriguez, *Classical and Quantum Distinctions between Weak and Strong Coupling*, Eur. J. Phys. **37**, 025802 (2016). https://doi.org/10.1088/0143-0807/37/2/025802.

[18] Y.-Y. Cai, E. Sung, R. Zhang, L. J. Tauzin, J. G. Liu, B. Ostovar, Y. Zhang, W.-S. Chang, P. Nordlander, and S. Link, *Anti-Stokes Emission from Hot Carriers in Gold Nanorods*, Nano Lett. **19**, 1067 (2019). https://doi.org/10.1021/acs.nanolett.8b04359.

[19] Y. Dubi, Y. Sivan, *"Hot" electrons in metallic nanostructures - nonthermal carriers or heating?*, Light Sci. Appl. **8**, 828-835 (2019). https://doi.org/10.1038/s41377-019-0199-x.

[20] K.-Q. Lin, J. Yi, S. Hu, J.-J. Sun, J.-T. Zheng, X. Wang, and B. Ren, *Intraband Hot-Electron Photoluminescence from Single Silver Nanorods*, ACS Photonics **3**, 1248 (2016). https://doi.org/10.1021/acsphotonics.6b00238.

[21] S. Liu, A. Hammud, I. Hamada, M. Wolf, M. Müller, and T. Kumagai, *Nanoscale Coherent Phonon Spectroscopy*, Sci. Adv. **8**, eabq5682 (2022). https://doi.org/10.1126/sciadv.abq5682.

[22] W. Luo, B. G. Whetten, V. Kravtsov, A. Singh, Y. Yang, D. Huang, X. Cheng, T. Jiang, A. Belyanin, and M. B. Raschke, *Ultrafast Nanoimaging of Electronic Coherence of Monolayer WSe_2*, Nano Lett. **23**, 1767-1773 (2023). https://doi.org/10.1021/acs.nanolett.2c04536.